

Point Cloud Matters: Rethinking the Impact of Different Observation Spaces on Robot Learning

Haoyi Zhu^{1,2} Yating Wang^{1,3} Di Huang¹ Weicai Ye^{1,4} Wanli Ouyang¹ Tong He¹

Abstract

In this study, we explore the influence of different observation spaces on robot learning, focusing on three predominant modalities: RGB, RGB-D, and point cloud. Through extensive experimentation on over 17 varied contact-rich manipulation tasks, conducted across two benchmarks and simulators, we have observed a notable trend: point cloud-based methods, even those with the simplest designs, frequently surpass their RGB and RGB-D counterparts in performance. This remains consistent in both scenarios: training from scratch and utilizing pretraining. Furthermore, our findings indicate that point cloud observations lead to improved policy zero-shot generalization in relation to various geometry and visual clues, including camera viewpoints, lighting conditions, noise levels and background appearance. The outcomes suggest that 3D point cloud is a valuable observation modality for intricate robotic tasks. We will open-source all our codes and checkpoints, hoping that our insights can help design more generalizable and robust robotic models.

1 Introduction

The evolution of robot learning has been profoundly influenced by the integration of visual observations, a cornerstone that enables robots to perceive and interact with complex environments. A key challenge faced by contemporary robot models lies in their limited generalization ability, especially in dynamic and intricate settings.

Commonly, robotic vision has predominantly utilized 2D images (Radosavovic et al., 2023; Parisi et al., 2022; Ma et al., 2022; Nair et al., 2023; Majumdar et al., 2023; Brohan et al., 2022; Zhao et al., 2023; Chi et al., 2023) for their sim-

¹Shanghai Artificial Intelligence Laboratory ²University of Science and Technology of China ³Northwestern Polytechnical University ⁴Zhejiang University. Correspondence to: Tong He <hetong@pjlab.org.cn>.

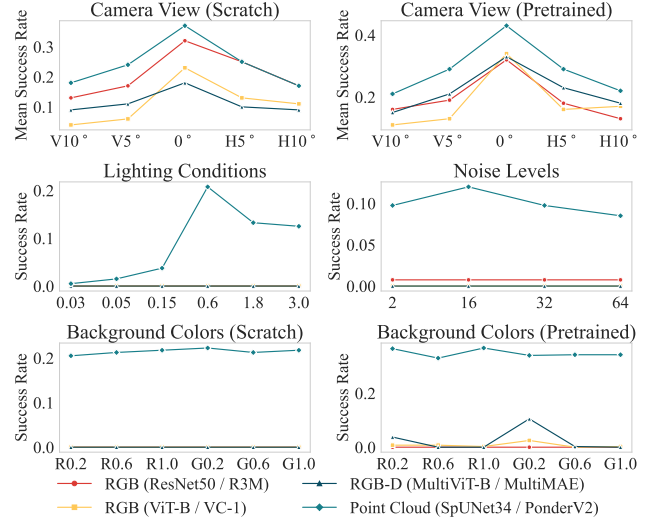


Figure 1. Point cloud has better zero-shot generalization ability on camera view and visual changes. *First row:* Zero-shot camera view generalization of different observations with training-from-scratch encoders (*left*) and with SOTA PVRs (*right*). *Second row:* Zero-shot generalization on different unseen lighting conditions (*left*) and rendering noise levels (*right*). *Third row:* Zero-shot results, with different background colors, of training-from-scratch encoders (*left*) and PVRs (*right*). Detailed explanation and analysis can be found in Sec. 6.

plicity and the considerable advancements in 2D foundation models (He et al., 2020; Bao et al., 2021; Radford et al., 2021; He et al., 2022). For instance, RT-1 (Brohan et al., 2022) has leveraged RGB images from extensive real-world task datasets. Action Chunking Transformer (ACT) (Zhao et al., 2023) employs multiple RGB cameras to inform its transformer policy. Despite their ubiquity, RGB images often fall short of accurately capturing the three-dimensional structure of environments, essential for precise action execution. These methods also exhibit vulnerable generalization to changes such as lighting conditions and camera viewpoints, owing to their reliance on appearance.

Given that the actions of robot policies derived from observations are typically three-dimensional in either Cartesian spaces or joint spaces, integrating 3D information into observation spaces appears inherently reasonable. For example, methods like CLIPort (Shridhar et al., 2022) incorporate depth images for enhanced task execution, while

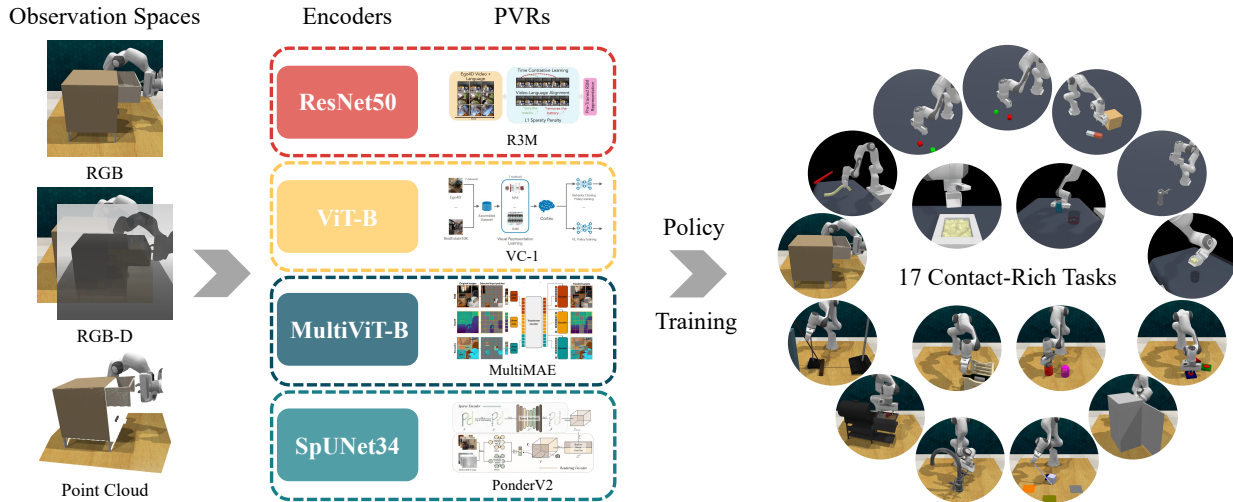


Figure 2. Overview of this work. We examine the impact of various observation spaces, specifically RGB, RGB-D, and point clouds, on robot learning. For this evaluation, we select prevalent and state-of-the-art methods, along with pretrained representations, and use them to train an action chunking transformer-based policy network. This approach is assessed across 17 contact-rich tasks using two extensively utilized simulators and benchmarks.

others such as Perceiver-Actor (Shridhar et al., 2023) and ACT3D (Gervet et al., 2023) transform RGB-D images into point clouds for explicit spatial information. Nevertheless, which modality is more suitable for robotic tasks remains unexplored due to the absence of a unified comparative framework across these modalities in the existing literature.

In this paper, we select three modalities that are widely used in robotic tasks: RGB, RGB-D, and 3D point cloud. RGB images are readily available and supported by robust pretrained visual representations (PVRs). RGB-D images associate it with extra depth information. Point cloud, on the other hand, provides precise spatial cues. To make a fair comparison, we avoid complex designs and domain-specific techniques but instead opt for simple, commonly accepted designs in each modality community. Our aim is to derive meaningful insights from more challenging tasks, beyond the scope of easy settings often explored in previous works. Therefore, rather than employing a basic 2- or 3-layer MLP as commonly done (Nair et al., 2023; Radosavovic et al., 2023; Hansen et al., 2022; Majumdar et al., 2023), we utilize Action Chunking Transformer (Zhao et al., 2023) as the controller to assess various observation spaces across 17 contact-rich tasks in two well-known, realistic, and challenging benchmarks and simulators: ManiSkill2 (Gu et al., 2023) and RL Bench (James et al., 2020).

We first evaluate each observation space under identical settings, differing only in input modality and corresponding encoders. Recognizing the growing prevalence and varied efficacy of pretrained visual representations (PVRs) across different modalities, we also investigate the performance of state-of-the-art PVRs within each observation space. Additionally, we also focus on the zero-shot generalization

capabilities regarding camera viewpoints, lighting conditions, visual appearance, and sample efficiency.

To the best of our knowledge, our work is the first to undertake such an extensive comparison of different observation spaces. Our key findings can be summarized as follows:

- Point cloud emerges as a promising observation modality for robot learning. Simple point cloud baselines exhibit the highest mean success rate and mean rank, both from scratch and with pretraining.
- Point cloud demonstrates more robustness to camera view and visual changes, sometimes generalizing effectively even under significant viewpoint alterations.

2 Methods

Comparing different observation spaces convincingly is a non-trivial task. Avoiding complex or niche tricks, we adopt the most recognized and state-of-the-art (SOTA) methods across various observation domains. An overview of the encoders and PVRs used is presented in Tab. 1.

2.1 Problem Formulation

The fundamental aim of robot learning is to develop a policy, $\pi(\cdot|o_t, \tau)$, deriving actions from visual observations. Here, $o_t \in \mathcal{O}$ is the observation at time t , and τ represents an optional task-specific target. The robot, guided by this policy, executes an action $a_t \in \mathcal{A}$, generating new observations and receiving a binary reward $r \in \{0, 1\}$ at each episode’s end. Our goal is to maximize expected rewards, considering task distribution, initial observations, and transition dynamics.

Table 1. Overview of encoders and corresponding PVRs. #Params denotes number of model parameters while #Pretrained represents number of images or point clouds during pretraining.

Obs. Space	Encoder	#Params	PVR	#Pretrained
RGB	○ ResNet50	23.5M	● R3M	5M
	○ ViT-B	85.8M	● VC-1	5.6M
RGB-D	○ MultiViT-B	86.1M	● MultiMAE	1.28M
Point Cloud	○ SpUNet34	43.6M	● PonderV2	4.5K

Observation Space. We analyze in detail the observation spaces \mathcal{O} , emphasizing that observations o_t are projections of the real world $w_t \in \mathcal{W}$ via different sensors $h(\cdot) : \mathcal{W} \rightarrow \mathcal{O}$. Our policy, therefore, is $\pi_h(\cdot | o_t = h(w_t), \tau)$. We explore the diversity of h , focusing on three observation spaces: \mathcal{O}_{RGB} , $\mathcal{O}_{\text{RGB-D}}$, and \mathcal{O}_{PCD} .

Representation Space. Visuo-motor policies often use an encoder, \mathcal{F}_θ , to transform o_t into a state representation $\hat{s} = \mathcal{F}_\theta(o_t)$. The policy then becomes $\pi(\cdot | \hat{s}, \tau)$, with $\hat{s} = \mathcal{F}_\theta(o_t)$ and $o_t = h(w_t)$. While previous studies (Nair et al., 2023; Radosavovic et al., 2023; Hansen et al., 2022; Majumdar et al., 2023) have primarily focused on pretrained RGB image encoders, our research evaluates various pretraining methods across different observation types.

Behavior Cloning. We adopt behavior cloning (Pomerleau, 1988; Levine et al., 2016; Zhang et al., 2018) for policy learning due to its simplicity and universality. This method trains π on a dataset \mathcal{D} of successful demonstrations. The objective is to align the robot’s actions with these demonstrations by optimizing π to minimize the negative log-likelihood of the actions based on the observations and goal conditions.

2.2 Encoders

RGB Observation. For RGB images, we utilize ○ ResNet50 (He et al., 2016) and ○ ViT-B (Dosovitskiy et al., 2020), the two most popular image encoders.

RGB-D Observation. ○ MultiViT-B (Bachmann et al., 2022), a Vision Transformer variant, is used for RGB-D observations. This model is designed for multi-modal inputs with distinct projection layers. It can effectively integrate RGB data with depth information.

Point Cloud Observation. For point cloud, we select SparseUNet34 (○ SpUNet34) (Contributors, 2022), which is a sparse convolutional network. It is widely adopted in the 3D vision community for point cloud perception tasks.

Feature Extraction. Feature extraction approaches vary by encoder: ResNet uses final layer features while ViT and MultiViT employ the [CLS] token. Regarding SpUNet baselines, we simply use farthest point sampling (FPS) (Eldar et al., 1997; Qi et al., 2017) and K-nearest neighborhood (KNN) (Duda et al., 1973; Cover & Hart, 1967). Specifi-

cally, on the final 3D sparse convolutional feature map, we first use FPS to select S seed points, then employ KNN to form S clusters around the seeds. These clusters undergo a linear projection and pooling layer, resulting in S features as inputs for the policy network. Our aim is to apply simple and common methods to facilitate a fair comparison.

2.3 Pretrained Visual Representations

In our study, we utilize publicly available model weights for the following pretraining methods:

RGB PVR. ● R3M (Nair et al., 2023) and ● VC-1 (Majumdar et al., 2023) are used for ○ ResNet50 and ○ ViT-B, respectively. Both are acclaimed in the realm of Embodied AI. R3M (Nair et al., 2023) mainly leverages time-contrastive learning and video-language alignment to pre-train on Ego4D (Grauman et al., 2022) dataset. VC-1 pre-trains a ViT using a masked auto-encoding (MAE) (He et al., 2022) approach with a broad training scope, encompassing a combination of multiple sources such as Ego4D (Grauman et al., 2022) and ImageNet (Deng et al., 2009), etc.

RGB-D PVR. We selected Multi-modal Multi-task Masked Autoencoders (● MultiMAE) (Bachmann et al., 2022) as the PVR of ○ MultiViT for RGB-D images. MultiMAE (Bachmann et al., 2022) is jointly pretrained on RGB, depth, and semantic modalities using masked autoencoding (He et al., 2022) on the pseudo-labeled ImageNet-1K dataset (Deng et al., 2009). We focus on its RGB and depth components.

Point Cloud PVR. For point cloud data, we adopt ● PonderV2 (Zhu et al., 2023), the SOTA self-supervised learning method for point cloud. It pretrains an ○ SpUNet via differentiable neural rendering on 3 point cloud datasets.

2.4 Policy Network

In this research, we explore non-trivial, contact-rich tasks to derive meaningful insights. To avoid bottlenecks in policy learning, we diverge from previous approaches (Parisi et al., 2022; Nair et al., 2023; Radosavovic et al., 2023; Hansen et al., 2022; Majumdar et al., 2023) of using shallow 2- or 3-layer MLPs, common in 2D PVR studies. Instead, we employ the **Action Chunking Transformer (ACT)** (Zhao et al., 2023) as our policy network. ACT (Zhao et al., 2023) models behavior cloning using a conditional VAE (Sohn et al., 2015) and has demonstrated remarkable success in a variety of fine-grained manipulation tasks, both in simulated and real-world settings. See Appendix B for more details.

3 Experimental Setup

Benchmarks and Simulators. Our study employs two well-known simulators and benchmarks, ManiSkill2 (Gu et al., 2023) and RL Bench (James et al., 2020), to evaluate the

Table 2. Results on different observation spaces. *M.S.* denotes Mean Success, while *M.R.* denotes Mean Rank.

Tasks	○ ResNet50	○ ViT-B	○ MultiViT-B	○ SpUNet34	
<i>ManiSkill2</i>					
PickCube	0.60	0.15	0.02	0.74	
StackCube	0.32	0.00	0.00	0.22	
TurnFaucet	0.49	0.27	0.35	0.39	
Peg-Insertion-Side	Grasp	0.73	0.36	0.16	0.81
	Align	0.18	0.02	0.01	0.28
	Insert	0.01	0.00	0.00	0.01
Excavate	0.02	0.00	0.00	0.11	
Hang	0.86	0.80	0.78	0.80	
Pour	0.07	0.00	0.00	0.10	
Fill	0.79	0.30	0.76	0.66	
<i>RLBench</i>					
open drawer	0.00	0.16	0.20	0.44	
sweep to dustpan of size	0.72	0.80	0.68	0.90	
meat off grill	0.24	0.16	0.00	0.72	
turn tap	0.00	0.00	0.00	0.00	
reach and drag	0.32	0.28	0.04	0.20	
put money in safe	0.60	0.76	0.28	0.60	
push buttons	0.12	0.40	0.12	0.04	
close jar	0.04	0.00	0.00	0.04	
place wine at rack location	0.00	0.00	0.00	0.00	
Mean Success Rate ↑	0.32	0.23	0.18	0.37	
Mean Rank ↓	1.74	2.47	2.89	1.58	

impact of different observation spaces in robotic learning. ManiSkill2 is recognized for its realistic physical simulation, while RLBench offers a range of vision-guided, language-conditioned tasks. We selected 17 diverse, contact-rich tasks (8 from ManiSkill2 and 9 from RLBench), listed in Tab. 2. The tasks are selected following prior works (Jia et al., 2023; Shridhar et al., 2023) and we remove those tasks on which all methods have 0 success rates. Detailed descriptions and examples of each task can be found in Appendix A.

Evaluation Metrics. For each task, we employ success rate to evaluate the performance of each method. In addition, we adopt the evaluation methodology from VC-1 (Majumdar et al., 2023) encompassing two key metrics: **Mean Success** and **Mean Rank**. *Mean Success* calculates the average success rate across all tasks, providing an overall performance indicator. *Mean Rank*, on the other hand, involves ranking each method based on their success rate for each task and then averaging these rankings across all tasks. This metric offers insights into the relative performance of methods across diverse tasks.

Training and Evaluation Details. In ManiSkill2 (Gu et al., 2023) experiments, each model is trained using the demonstrations provided by the official ManiSkill2 challenge. For TurnFaucet-v0, we adhere to the protocol outlined by Jia et al. (2023), utilizing 10 faucet models. For PegInsertionSide-v0, we also report the results for each sub-stage (*i.e.* grasp, align, and insert), following Jia et al. (2023). We take only the base camera with resolution of 128×128 for inputs. We evaluate each ManiSkill2 task using 400 fixed random seeds. In the RLBench (James et al., 2020) experiments, following the settings of PerAct (Shrid-

Table 3. Results of PVRs on different observation spaces. Blue and red numbers denote the relative performance changes compared to their corresponding training-from-scratch encoders.

Tasks	● R3M	● VC-1	● MultiMAE	● PonderV2	
<i>ManiSkill2</i>					
PickCube	0.82 ^{↑0.22}	0.77 ^{↑0.63}	0.52 ^{↑0.49}	0.87 ^{↑0.13}	
StackCube	0.41 ^{↑0.09}	0.06 ^{↑0.06}	0.30 ^{↑0.30}	0.35 ^{↑0.13}	
TurnFaucet	0.46 ^{↓0.03}	0.42 ^{↑0.15}	0.37 ^{↑0.02}	0.27 ^{↓0.12}	
Peg-Insertion-Side	Grasp	0.84 ^{↑0.11}	0.63 ^{↑0.27}	0.71 ^{↑0.55}	0.65 ^{↓0.17}
	Align	0.23 ^{↑0.06}	0.07 ^{↑0.05}	0.15 ^{↑0.14}	0.23 ^{↑0.05}
	Insert	0.01 ^{↑0.01}	0.00 ^{↑0.00}	0.01 ^{↑0.01}	0.02 ^{↑0.01}
Excavate	0.38 ^{↑0.36}	0.20 ^{↑0.20}	0.28 ^{↑0.28}	0.38 ^{↑0.27}	
Hang	0.84 ^{↓0.02}	0.84 ^{↑0.04}	0.77 ^{↓0.01}	0.83 ^{↑0.04}	
Pour	0.12 ^{↑0.06}	0.04 ^{↑0.04}	0.00 ^{↑0.00}	0.11 ^{↑0.02}	
Fill	0.88 ^{↑0.09}	0.78 ^{↑0.48}	0.68 ^{↓0.08}	0.73 ^{↑0.17}	
<i>RLBench</i>					
open drawer	0.00 ^{↑0.00}	0.24 ^{↑0.08}	0.36 ^{↑0.16}	0.60 ^{↑0.16}	
sweep to dustpan of size	0.52 ^{↓0.20}	0.96 ^{↑0.16}	1.00 ^{↑0.32}	0.96 ^{↑0.06}	
meat off grill	0.04 ^{↓0.20}	0.12 ^{↓0.04}	0.04 ^{↑0.04}	0.72 ^{↑0.00}	
turn tap	0.00 ^{↑0.00}	0.04 ^{↑0.04}	0.08 ^{↑0.08}	0.00 ^{↑0.00}	
reach and drag	0.04 ^{↓0.28}	0.20 ^{↓0.08}	0.16 ^{↑0.12}	0.28 ^{↑0.08}	
put money in safe	0.48 ^{↓0.12}	0.72 ^{↓0.04}	0.56 ^{↑0.28}	0.64 ^{↑0.04}	
push buttons	0.24 ^{↑0.12}	0.44 ^{↑0.04}	0.48 ^{↑0.36}	0.16 ^{↑0.12}	
close jar	0.08 ^{↑0.04}	0.08 ^{↑0.08}	0.00 ^{↑0.00}	0.28 ^{↑0.24}	
place wine at rack location	0.00 ^{↑0.00}	0.00 ^{↑0.00}	0.08 ^{↑0.08}	0.16 ^{↑0.16}	
Mean Success Rate ↑	0.32 ^{↑0.00}	0.34 ^{↑0.10}	0.33 ^{↑0.15}	0.43 ^{↑0.06}	
Mean Rank ↓	2.37 ^{↑0.63}	2.63 ^{↑0.16}	2.68 ^{↓0.21}	1.89 ^{↑0.32}	

har et al., 2023), we train each task with 100 demonstrations and test them on 25 distinct, held-out scenes. Similarly, only a front camera with 128×128 resolution is used. Across all experiments, we adopt an AdamW (Loshchilov & Hutter, 2017) optimizer with the OneCycle (Smith & Topin, 2019) learning rate scheduler. Each method is trained with learning rates of $1e-5$, $5e-5$, and $1e-4$. The checkpoint with lowest validation loss is selected for evaluation. Further implementation details, experimental procedures and hyperparameter settings are available in Appendix C.

4 How do varying observation spaces influence robot learning performance?

Our initial investigation focuses on assessing the task performance across different observation spaces. Each encoder is trained from scratch on individual tasks, utilizing identical training data across all modalities except for the input observation types. As shown in Tab. 2, ○ SpUNet34 ranks highest for 8 times, and ○ ResNet50 ranks highest for 5 times. ○ MultiViT performs the worst (only 0.18 on average). Although depth images contain pseudo spatial clues, the explicit representation of the 3D point cloud shows superiority on the majority of the tasks. The results also reveal that no single observation modality consistently outperforms others across all tasks. However, it is notable that the point cloud encoder, ○ SpUNet34, achieves the highest mean success rate (0.37) and mean rank (1.58) overall. This suggests that *point cloud, on average, possesses significant potential*

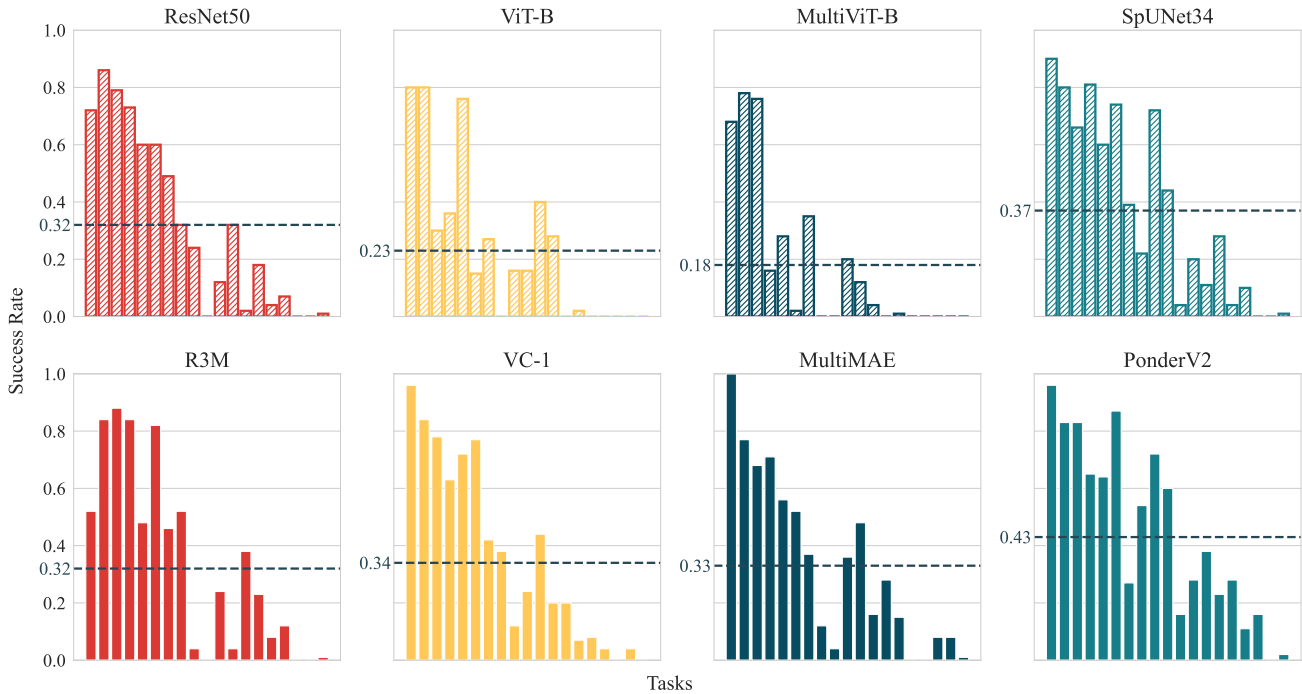


Figure 3. Performance distributions of different methods. The first row shows the results of different encoders of different observation spaces trained from scratch while the second row shows the performance of their corresponding state-of-the-art pretrained visual representations. The tasks are sorted by average success rate across all methods. Therefore, tasks on the right side can be seen as more difficult. The dark cyan dashed line denotes the mean success rate across all tasks. We can see that point cloud-based methods, whether trained from scratch or with pretrained, have a higher mean success rate and are better at difficult tasks.

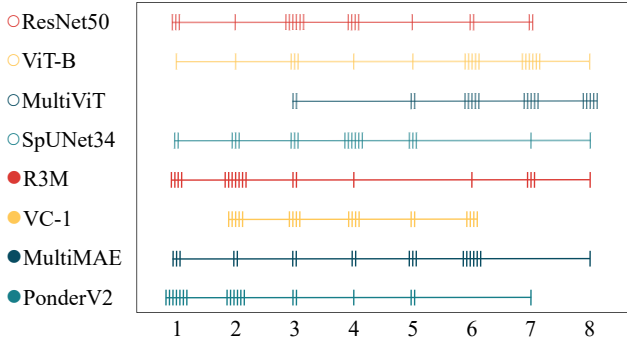


Figure 4. Overall rank distribution per method. For every method, we compute the overall ranks it achieved on all tasks. For example, ● PonderV2 ranks 1st on 7 tasks.

in the realm of robotic learning tasks.

Moreover, both ● ViT-B and ● MultiViT-B show notably lower performance (mean success rate of 0.23 and 0.18). This finding aligns with existing literature in computer vision (Raghu et al., 2021; d’Ascoli et al., 2021), suggesting that *Vision Transformers may not be well-suited for training from scratch on small-scale datasets.*

For further analysis, we sort tasks based on their average success rate across different methods, as depicted in the first row of Fig. 3. This visualization of performance distributions offers insights into the relative difficulty of each

task and the efficacy of each encoder modality. Notably, the superiority of ● SpUNet34 becomes more apparent in tasks of *moderate and higher difficulty levels*. This trend suggests that point cloud encoders may offer distinct advantages in complex scenarios, potentially due to their inherent capacity to capture detailed spatial information.

5 What is the performance impact of PVRs in these diverse observation spaces?

A pivotal advancement in modern computer vision, particularly for RGB images, is the development of pretrained visual representations (PVRs). These have significantly improved performance in downstream tasks, including embodied AI and robotics (Nair et al., 2023; Ma et al., 2022; Radosavovic et al., 2023; Hansen et al., 2022; Majumdar et al., 2023). In our experiments, we utilize publicly available weights for the corresponding encoders to assess the impact of SOTA PVRs across different observation spaces.

Consistent with prior studies (Hansen et al., 2022; Majumdar et al., 2023), our findings indicate that maintaining PVRs in a frozen state throughout training tends to yield inferior results compared to encoders trained from scratch, likely as a result of a significant domain gap from the training data. However, contrary to some findings of Hansen et al. (2022), our experiments indicate that straightforward end-to-end

finetuning is effective across most tasks without any specific tricks. We attribute this to the more realistic nature of our environments, which presumably narrows the domain gap.

Results with finetuned PVRs are summarized in Tab. 3. While ● R3M enhances performance in many tasks, its performance drops on 6 tasks, thus leading to an almost negligible increase in mean success rate. Notably, ViTs exhibit significant improvement with appropriate pretraining. Both ● VC-1 and ● MultiMAE, leveraging the Masked Autoencoder (MAE) pretraining paradigm, show the most substantial average improvements (0.10 and 0.15 respectively). ● PonderV2, although demonstrating slightly lesser average gains of 0.06, which may be caused by the limited pretraining data, still *maintains the best performance in terms of mean success rate and rank*. This underscores the efficacy of point cloud observation spaces and highlights the potential for further advancements in point cloud PVRs.

To gain a broader perspective on the overall rank performance of all methods, we combine the rankings of both train-from-scratch and pretrained encoders. As illustrated in Fig. 4, RGB-D observations are unsatisfactory when trained from scratch, unless with a strong pretraining. What’s more, *PVRs are generally critical, and point cloud encoders, especially when pretrained, stand out as notably promising within the range of observation spaces*.

6 Evaluating Zero-Shot Generalization Capabilities Across Observation Spaces

A key objective in robot learning is to build an agent with strong zero-shot generalization abilities. This section extensively evaluates the zero-shot generalization capabilities of different observation spaces, focusing on camera view (Sec. 6.1) and visual changes (Sec. 6.2). Note that the RGB color is included in the feature of point clouds.

6.1 Zero-Shot Generalization to Camera View

Camera view generalization is crucial yet challenging for robot learning models, as deploying a robot with the exact training camera positions is often impractical. Camera view disturbance is extremely challenging since it can lead to huge geometry changes. Despite its importance, this aspect is often overlooked in prior works. Our study emphasizes the need for robust camera view generalization. Given that the camera is fixed during training, we conduct zero-shot evaluations across novel camera viewpoints, moving vertically and horizontally by 5° and 10° respectively.

The mean success rates under these varied camera views are presented in Tab. 4 and visually represented in Fig. 1. All methods are significantly affected by geometry changes caused by camera views, even with only 5 degrees. The results highlight a prevalent sensitivity to camera view alter-

Table 4. Mean success rate on zero-shot camera view changes.

Methods	Vertical		Horizontal		Average
	5°	10°	5°	10°	
○ ResNet50	0.17	0.13	0.25	0.17	0.18
○ ViT-B	0.06	0.04	0.13	0.11	0.09
○ MultiViT	0.11	0.09	0.10	0.09	0.10
○ SpUNet34	0.24	0.18	0.25	0.17	0.21
● R3M	0.19	0.16	0.18	0.13	0.16
● VC-1	0.13	0.11	0.16	0.17	0.14
● MultiMAE	0.21	0.15	0.23	0.18	0.19
● PonderV2	0.29	0.21	0.29	0.22	0.25

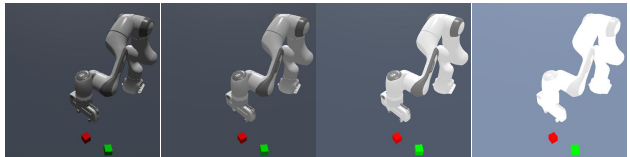


Figure 5. Examples of different lighting conditions. The light intensities are 0.03, 0.6, 0.15, 0.3 from left to right respectively.

ations in current robot models. However, *leveraging point cloud data, both pretrained and from scratch, shows notable resilience to these geometry changes*.

This observation raises critical considerations. It appears that image-based models are more likely to be overly attuned to specific training camera views or geometries, suggesting a possible overfitting rather than a genuine understanding of action space skills. Many algorithms such as Zhao et al. (2023); Chi et al. (2023) are evaluated using identical camera setups as in training, leaving their true robustness untested. The task of inferring 3D positions or rotations from images without camera parameters is inherently ill-posed to some extent. Thus, our findings suggest that further exploration into point cloud representations could be pivotal in developing more generalizable, camera view-robust robot models.

6.2 Zero-Shot Generalization to Visual Changes

Our previous analysis reveals that while point cloud methods generally excel, they do not uniformly outperform in all tasks. Following our camera view generalization study, a pertinent question arises: *Do RGB and RGB-D approaches truly excel in performance, or is their advantage claimed by a tendency to overfit?* To address this question, the StackCube task was selected for its complexity and apparent preference for the RGB modality, as demonstrated by its higher initial accuracy. As demonstrated in Fig. 1, we observe that ○ SpUNet34, when compared in a zero-shot generalization scenario involving diverse visual changes, is surpassed by the performance of ○ ResNet50.

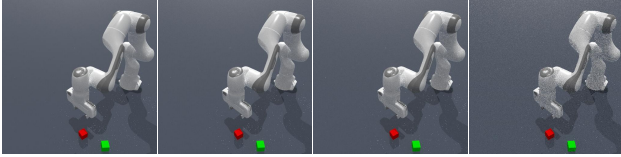


Figure 6. **Examples of different noise levels.** The ray tracing samples per pixel are 64, 32, 16, 2 from left to right respectively.

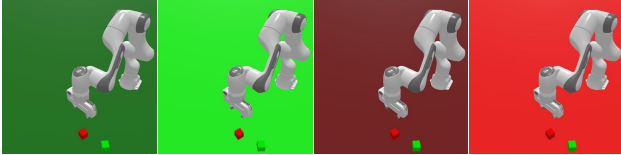


Figure 7. **Examples of different background colors.** The background color is denoted as ‘G0.2’, ‘G1.0’, ‘R0.2’, ‘R1.0’ from left to right respectively, where ‘G’ and ‘R’ means green or red and the number represents the value of green or red channel.

Zero-Shot Generalization to Lighting Conditions. A primary visual condition we assess is lighting, a common variable in real-world applications. For instance, a model trained in the morning might be deployed under evening lighting conditions. We simulate such scenarios by varying lighting intensity, testing it at levels of 0.03, 0.05, 0.15, 0.6, 1.8, 3, from the default intensity of 0.3. Visual illustrations of some lighting conditions are provided in Fig. 5 and the results are depicted on the left side of the second row in Fig. 1. It becomes evident that *RGB and RGB-D methods are significantly impacted by lighting changes, whereas the point cloud approach demonstrates a higher degree of robustness.* Notably, *darker lighting conditions pose a greater challenge to robotic models.* This observation underscores the vulnerability of RGB and RGB-D methods to environmental lighting variations, highlighting the resilience of point cloud methods in such scenarios.

Zero-Shot Generalization to Visual Noise. In real-world deployments, noise is an unavoidable factor, often resulting from hardware inaccuracies or environmental conditions. While simulators typically operate in noise-free settings, we introduce visual noise to mimic real-world scenarios. This is achieved by switching the rendering mode from default rasterization to ray tracing, disabling the denoiser, and varying the number of ray tracing samples per pixel, thus altering the noise level. We evaluate four distinct noise levels, corresponding to 2, 16, 32, and 64 ray tracing samples per pixel. Visualizations of these noise levels are presented in Fig. 6. The outcomes of these tests are displayed on the right side of the second row in Fig. 1. Our research highlights a marked susceptibility of RGB and RGB-D methods to visual noise, leading to a significant decline in their performance when subjected to such conditions. In contrast, *point cloud-based methods exhibited remarkable robustness to noise.* This resilience of point cloud methods is particularly noteworthy, as it suggests their potential for more reliable performance

Table 5. **Sample efficiency results on RL Bench tasks.**

#Training	10	25	100
○ ResNet-50	0.009	0.009	0.305
○ ViT-B	0.000	0.040	0.239
○ MultiViT-B	0.004	0.027	0.190
○ SpUNet32	0.004	0.018	0.351
● R3M	0.009	0.067	0.317
● VC-1	0.000	0.040	0.348
● MultiMAE	0.000	0.031	0.334
● PonderV2	0.013	0.040	0.439

in noisy, real-world operational environments.

Zero-Shot Generalization to Background Colors. The ability to function across diverse background conditions is essential for the deployment of robots in real-world environments, where such conditions can change significantly. The original setting features a gray floor, which we alter to red and green, varying the ‘R’ or ‘G’ values to 0.2, 0.6, 1.0 respectively. Visual examples of these background color changes are illustrated in Fig. 7. The results, shown on the right side of Fig. 1, align with our previous observations: *point cloud methods exhibit better robustness when it comes to adapting to background color variations.*

For comprehensive results on all our generalization experiments, we invite readers to consult Tab. 6, Tab. 7, Tab. 8, Tab. 9 and Tab. 10 in Appendix D. These findings underscore a significant insight: although RGB observations may excel in some tasks, they *lack robustness against various geometry (camera view) and visual changes.* In contrast, while point cloud observation spaces may not universally outperform in all individual tasks, they *demonstrate markedly greater generalizability to a range of visual alterations and geometric changes.* This phenomenon can be attributed to the inherent nature of the data representation. 2D images predominantly rely on planar color values, whereas point clouds incorporate not only color but also explicit three-dimensional spatial information. This multidimensional data structure reduces overreliance on visual cues alone, a critical advantage in developing robust robot models. Consequently, point cloud emerges as a promising observation space for developing robot models with zero-shot adaptation to new environments.

7 How do different observation spaces and PVRs influence the sample efficiency?

To understand the sample efficiency of various observation spaces, we also conduct experiments with reduced training data on RL Bench tasks. Specifically, each method is trained using only 10 and 25 training samples. The outcomes of these experiments are shown in Tab. 5 and Appendix E. Our analysis reveals that point cloud observation spaces do

not exhibit a pronounced advantage in terms of sample efficiency compared to other modalities. Notably, our results indicate that *pretrained representations consistently bolster performance in scenarios with limited training data*. This suggests that leveraging pretrained models can be particularly beneficial in few-shot learning contexts, where the availability of extensive training datasets is constrained.

8 Related Work

Pretrained Visual Representations (PVRs). Self-supervised learning (SSL) in 2D and 3D computer vision has recently gained significant interest, utilizing various methods like contrastive learning (Chen et al., 2020; He et al., 2020; Chen et al., 2021; Xie et al., 2020; Hou et al., 2021; Wu et al., 2023; Radford et al., 2021), distillation-based technique (Caron et al., 2021; Baevski et al., 2022; Oquab et al., 2023)s, reconstructive approaches (Bao et al., 2021; He et al., 2022; Pang et al., 2022; Zhang et al., 2022; Yang et al., 2023a), and differentiable rendering for pre-training (Huang et al., 2023; Zhu et al., 2023; Yang et al., 2023b). This SSL progress has been integrated into Embodied AI and robot learning (Parisi et al., 2022; Nair et al., 2023; Radosavovic et al., 2023; Ma et al., 2022; Khandelwal et al., 2022; Yadav et al., 2022; Majumdar et al., 2023; Fan et al., 2022), showing impressive embodied task performance. However, most studies have focused on 2D RGB spaces, neglecting varied observation spaces and 3D perceptual representations (PVRs). Our research is pioneering in exploring the effects of different observation spaces and their corresponding PVRs.

Observation Spaces in Robot Learning. In robot learning, estimating accurate states from raw observations is challenging, with the predominant focus on 2D RGB image-based action mapping. However, the relevance of 3D information is increasingly recognized (Zeng et al., 2021; Gou et al., 2021; Shridhar et al., 2022; 2023; Gervet et al., 2023; Yen-Chen et al., 2020; Fang et al., 2023b; Li et al., 2022; Christen et al., 2023; Ze et al., 2023), as seen in methods like CLI-Port (Shridhar et al., 2022) and Perceiver-Actor (Shridhar et al., 2023). Despite these advancements, there’s a lack of systematic comparison between 2D and 3D methods, and some 3D techniques involve complex designs (Gervet et al., 2023; Li et al., 2022; Christen et al., 2023) or rely on dense voxel representations (Shridhar et al., 2023; Ze et al., 2023). Our work aims to provide a more equitable comparison of different observation spaces using simple and common techniques.

Robot Learning for Manipulation. Robot manipulation, often modeled as (Partially-Observable) Markov Decision Processes (Kaelbling et al., 1998; Kroemer et al., 2021), faces challenges in reinforcement learning (RL) (Sutton & Barto, 1999; Finn & Levine, 2017; Gu et al., 2017; Schenk

& Fox, 2018) due to multi-objectiveness, non-stationarity, sim-to-real gaps, and poor sample efficiency (Kroemer et al., 2021). Behavior cloning (Pomerleau, 1988; Levine et al., 2016) has emerged as a successful alternative, with diverse approaches like Perceiver-Actor’s (Shridhar et al., 2023), RT-1 (Brohan et al., 2022), RT-2 (Brohan et al., 2023), VIMA (Jiang et al., 2023), *etc.* Additionally, models like the Action Chunking Transformer (Zhao et al., 2023) and diffusion policy (Chi et al., 2023) use generative models (conditional VAE (Sohn et al., 2015) and diffusion model (Ho et al., 2020)) for modeling human demonstrations. Recent foundational models like RT-X (Padalkar et al., 2023) and Octo (Team et al., 2023) primarily use RGB images for observation. Our research focuses on exploring the impact of different observation spaces, aiming to provide insights for future robot learning advancements.

9 Conclusion

Our investigation into the influence of diverse observation spaces on robot learning has led to several significant insights. We demonstrate that point cloud-based methods, even with simplest designs, consistently outperform their RGB and RGB-D counterparts in terms of both mean success rate and robustness to various geometry or visual factors like camera viewpoints, lighting conditions, noise levels and background colors. This superiority persists regardless of whether the methods are trained from scratch or with pretraining, underscoring the potential of point cloud as a promising observation modality in robotics.

Limitations and Future Work. While point cloud methods show promise, they exhibit limitations in sample efficiency. The burgeoning field of large-scale 3D datasets, such as RH20T (Fang et al., 2023a) and DL3DV-10K (Ling et al., 2023), presents an opportunity to scale up 3D PVR methods using these extensive datasets, which could potentially yield more robust and generalized solutions for robotic learning.

Our study employed simple designs, such as FPS, which risks over-sampling or full-sampling on background areas, potentially impacting policy learning. Future work could explore dynamic sampling techniques like cross-attention or object-centric representations to address this.

Additionally, this study focus on single modality scenarios. However, integrating multiple observation spaces using advanced multi-modal techniques could offer significant benefits. Extending beyond visual observation spaces to include modalities like tactile sensing also presents an intriguing avenue for research.

Finally, while our experiments are conducted on simulated benchmarks for consistency and fairness, efforts to test and adapt these findings in real-world scenarios are an essential step for future research in robot learning.

References

- Bachmann, R., Mizrahi, D., Atanov, A., and Zamir, A. Multima: Multi-modal multi-task masked autoencoders. In *European Conference on Computer Vision*, pp. 348–367. Springer, 2022.
- Baevski, A., Hsu, W.-N., Xu, Q., Babu, A., Gu, J., and Auli, M. Data2vec: A general framework for self-supervised learning in speech, vision and language. In *International Conference on Machine Learning*, pp. 1298–1312. PMLR, 2022.
- Bao, H., Dong, L., Piao, S., and Wei, F. Beit: Bert pre-training of image transformers. *arXiv preprint arXiv:2106.08254*, 2021.
- Brohan, A., Brown, N., Carbajal, J., Chebotar, Y., Dabis, J., Finn, C., Gopalakrishnan, K., Hausman, K., Herzog, A., Hsu, J., et al. Rt-1: Robotics transformer for real-world control at scale. *arXiv preprint arXiv:2212.06817*, 2022.
- Brohan, A., Brown, N., Carbajal, J., Chebotar, Y., Chen, X., Choromanski, K., Ding, T., Driess, D., Dubey, A., Finn, C., et al. Rt-2: Vision-language-action models transfer web knowledge to robotic control. *arXiv preprint arXiv:2307.15818*, 2023.
- Caron, M., Touvron, H., Misra, I., Jégou, H., Mairal, J., Bojanowski, P., and Joulin, A. Emerging properties in self-supervised vision transformers. In *Proceedings of the IEEE/CVF international conference on computer vision*, pp. 9650–9660, 2021.
- Chen, T., Kornblith, S., Norouzi, M., and Hinton, G. A simple framework for contrastive learning of visual representations. In *International conference on machine learning*, pp. 1597–1607. PMLR, 2020.
- Chen, X., Xie, S., and He, K. An empirical study of training self-supervised vision transformers. *arXiv preprint arXiv:2104.02057*, 2021.
- Chi, C., Feng, S., Du, Y., Xu, Z., Cousineau, E., Burchfiel, B., and Song, S. Diffusion policy: Visuomotor policy learning via action diffusion. *arXiv preprint arXiv:2303.04137*, 2023.
- Christen, S., Yang, W., Pérez-D’Arpino, C., Hilliges, O., Fox, D., and Chao, Y.-W. Learning human-to-robot handovers from point clouds. In *Proceedings of the IEEE/CVF Conference on Computer Vision and Pattern Recognition*, pp. 9654–9664, 2023.
- Contributors, S. Spconv: Spatially sparse convolution library. <https://github.com/traveller59/spconv>, 2022.
- Cover, T. and Hart, P. Nearest neighbor pattern classification. *IEEE transactions on information theory*, 13(1):21–27, 1967.
- Damen, D., Doughty, H., Farinella, G. M., Fidler, S., Furnari, A., Kazakos, E., Moltisanti, D., Munro, J., Perrett, T., Price, W., et al. Scaling egocentric vision: The epic-kitchens dataset. In *Proceedings of the European conference on computer vision (ECCV)*, pp. 720–736, 2018.
- Deng, J., Dong, W., Socher, R., Li, L.-J., Li, K., and Fei-Fei, L. Imagenet: A large-scale hierarchical image database. In *2009 IEEE conference on computer vision and pattern recognition*, pp. 248–255. Ieee, 2009.
- Dosovitskiy, A., Beyer, L., Kolesnikov, A., Weissenborn, D., Zhai, X., Unterthiner, T., Dehghani, M., Minderer, M., Heigold, G., Gelly, S., et al. An image is worth 16x16 words: Transformers for image recognition at scale. *arXiv preprint arXiv:2010.11929*, 2020.
- Duda, R. O., Hart, P. E., et al. *Pattern classification and scene analysis*, volume 3. Wiley New York, 1973.
- d’Ascoli, S., Touvron, H., Leavitt, M. L., Morcos, A. S., Biroli, G., and Sagun, L. Convit: Improving vision transformers with soft convolutional inductive biases. In *International Conference on Machine Learning*, pp. 2286–2296. PMLR, 2021.
- Eldar, Y., Lindenbaum, M., Porat, M., and Zeevi, Y. Y. The farthest point strategy for progressive image sampling. *IEEE Transactions on Image Processing*, 6(9): 1305–1315, 1997.
- Fan, L., Wang, G., Jiang, Y., Mandlekar, A., Yang, Y., Zhu, H., Tang, A., Huang, D.-A., Zhu, Y., and Anandkumar, A. Minedojo: Building open-ended embodied agents with internet-scale knowledge. *Advances in Neural Information Processing Systems*, 35:18343–18362, 2022.
- Fang, H.-S., Fang, H., Tang, Z., Liu, J., Wang, J., Zhu, H., and Lu, C. Rh20t: A robotic dataset for learning diverse skills in one-shot. *arXiv preprint arXiv:2307.00595*, 2023a.
- Fang, H.-S., Wang, C., Fang, H., Gou, M., Liu, J., Yan, H., Liu, W., Xie, Y., and Lu, C. Anygrasp: Robust and efficient grasp perception in spatial and temporal domains. *IEEE Transactions on Robotics*, 2023b.
- Finn, C. and Levine, S. Deep visual foresight for planning robot motion. In *2017 IEEE International Conference on Robotics and Automation (ICRA)*, pp. 2786–2793. IEEE, 2017.

- Gervet, T., Xian, Z., Gkanatsios, N., and Fragkiadaki, K. Act3d: 3d feature field transformers for multi-task robotic manipulation. In *Conference on Robot Learning*, pp. 3949–3965. PMLR, 2023.
- Gou, M., Fang, H.-S., Zhu, Z., Xu, S., Wang, C., and Lu, C. Rgb matters: Learning 7-dof grasp poses on monocular rgb-d images. In *2021 IEEE International Conference on Robotics and Automation (ICRA)*, pp. 13459–13466. IEEE, 2021.
- Goyal, R., Ebrahimi Kahou, S., Michalski, V., Materzynska, J., Westphal, S., Kim, H., Haenel, V., Fruend, I., Yianilos, P., Mueller-Freitag, M., et al. The” something something” video database for learning and evaluating visual common sense. In *Proceedings of the IEEE international conference on computer vision*, pp. 5842–5850, 2017.
- Grauman, K., Westbury, A., Byrne, E., Chavis, Z., Furnari, A., Girdhar, R., Hamburger, J., Jiang, H., Liu, M., Liu, X., et al. Ego4d: Around the world in 3,000 hours of egocentric video. In *Proceedings of the IEEE/CVF Conference on Computer Vision and Pattern Recognition*, pp. 18995–19012, 2022.
- Gu, J., Xiang, F., Li, X., Ling, Z., Liu, X., Mu, T., Tang, Y., Tao, S., Wei, X., Yao, Y., et al. Maniskill2: A unified benchmark for generalizable manipulation skills. *arXiv preprint arXiv:2302.04659*, 2023.
- Gu, S., Holly, E., Lillicrap, T., and Levine, S. Deep reinforcement learning for robotic manipulation with asynchronous off-policy updates. In *2017 IEEE international conference on robotics and automation (ICRA)*, pp. 3389–3396. IEEE, 2017.
- Hansen, N., Yuan, Z., Ze, Y., Mu, T., Rajeswaran, A., Su, H., Xu, H., and Wang, X. On pre-training for visuomotor control: Revisiting a learning-from-scratch baseline. *arXiv preprint arXiv:2212.05749*, 2022.
- He, K., Zhang, X., Ren, S., and Sun, J. Deep residual learning for image recognition. In *Proceedings of the IEEE conference on computer vision and pattern recognition*, pp. 770–778, 2016.
- He, K., Fan, H., Wu, Y., Xie, S., and Girshick, R. Momentum contrast for unsupervised visual representation learning. In *Proceedings of the IEEE/CVF conference on computer vision and pattern recognition*, pp. 9729–9738, 2020.
- He, K., Chen, X., Xie, S., Li, Y., Dollár, P., and Girshick, R. Masked autoencoders are scalable vision learners. In *Proceedings of the IEEE/CVF conference on computer vision and pattern recognition*, pp. 16000–16009, 2022.
- Ho, J., Jain, A., and Abbeel, P. Denoising diffusion probabilistic models. *Advances in neural information processing systems*, 33:6840–6851, 2020.
- Hou, J., Graham, B., Nießner, M., and Xie, S. Exploring data-efficient 3d scene understanding with contrastive scene contexts. In *Proceedings of the IEEE/CVF Conference on Computer Vision and Pattern Recognition*, pp. 15587–15597, 2021.
- Huang, D., Peng, S., He, T., Yang, H., Zhou, X., and Ouyang, W. Ponder: Point cloud pre-training via neural rendering. In *Proceedings of the IEEE/CVF International Conference on Computer Vision*, pp. 16089–16098, 2023.
- James, S., Ma, Z., Arrojo, D. R., and Davison, A. J. Rlbench: The robot learning benchmark & learning environment. *IEEE Robotics and Automation Letters*, 5(2):3019–3026, 2020.
- Jia, Z., Liu, F., Thumhuri, V., Chen, L., Huang, Z., and Su, H. Chain-of-thought predictive control. *arXiv preprint arXiv:2304.00776*, 2023.
- Jiang, Y., Gupta, A., Zhang, Z., Wang, G., Dou, Y., Chen, Y., Fei-Fei, L., Anandkumar, A., Zhu, Y., and Fan, L. Vima: General robot manipulation with multimodal prompts. In *Fortieth International Conference on Machine Learning*, 2023.
- Kaelbling, L. P., Littman, M. L., and Cassandra, A. R. Planning and acting in partially observable stochastic domains. *Artificial intelligence*, 101(1-2):99–134, 1998.
- Khandelwal, A., Weihs, L., Mottaghi, R., and Kembhavi, A. Simple but effective: Clip embeddings for embodied ai. In *Proceedings of the IEEE/CVF Conference on Computer Vision and Pattern Recognition*, pp. 14829–14838, 2022.
- Kroemer, O., Niekum, S., and Konidaris, G. A review of robot learning for manipulation: Challenges, representations, and algorithms. *The Journal of Machine Learning Research*, 22(1):1395–1476, 2021.
- Levine, S., Finn, C., Darrell, T., and Abbeel, P. End-to-end training of deep visuomotor policies. *The Journal of Machine Learning Research*, 17(1):1334–1373, 2016.
- Li, Y., Li, S., Sitzmann, V., Agrawal, P., and Torralba, A. 3d neural scene representations for visuomotor control. In *Conference on Robot Learning*, pp. 112–123. PMLR, 2022.
- Ling, L., Sheng, Y., Tu, Z., Zhao, W., Xin, C., Wan, K., Yu, L., Guo, Q., Yu, Z., Lu, Y., et al. D13dv-10k: A large-scale scene dataset for deep learning-based 3d vision. *arXiv preprint arXiv:2312.16256*, 2023.

- Loshchilov, I. and Hutter, F. Decoupled weight decay regularization. *arXiv preprint arXiv:1711.05101*, 2017.
- Ma, Y. J., Sodhani, S., Jayaraman, D., Bastani, O., Kumar, V., and Zhang, A. Vip: Towards universal visual reward and representation via value-implicit pre-training. *arXiv preprint arXiv:2210.00030*, 2022.
- Majumdar, A., Yadav, K., Arnaud, S., Ma, Y. J., Chen, C., Silwal, S., Jain, A., Berges, V.-P., Abbeel, P., Malik, J., et al. Where are we in the search for an artificial visual cortex for embodied intelligence? *arXiv preprint arXiv:2303.18240*, 2023.
- Marcel, S. and Rodriguez, Y. Torchvision the machine-vision package of torch. In *Proceedings of the 18th ACM international conference on Multimedia*, pp. 1485–1488, 2010.
- Nair, S., Rajeswaran, A., Kumar, V., Finn, C., and Gupta, A. R3m: A universal visual representation for robot manipulation. In *Conference on Robot Learning*, pp. 892–909. PMLR, 2023.
- Oquab, M., Darcet, T., Moutakanni, T., Vo, H., Szafraniec, M., Khalidov, V., Fernandez, P., Haziza, D., Massa, F., El-Nouby, A., et al. Dinov2: Learning robust visual features without supervision. *arXiv preprint arXiv:2304.07193*, 2023.
- Padalkar, A., Pooley, A., Jain, A., Bewley, A., Herzog, A., Irpan, A., Khazatsky, A., Rai, A., Singh, A., Brohan, A., et al. Open x-embodiment: Robotic learning datasets and rt-x models. *arXiv preprint arXiv:2310.08864*, 2023.
- Pang, Y., Wang, W., Tay, F. E., Liu, W., Tian, Y., and Yuan, L. Masked autoencoders for point cloud self-supervised learning. In *European conference on computer vision*, pp. 604–621. Springer, 2022.
- Parisi, S., Rajeswaran, A., Purushwalkam, S., and Gupta, A. The unsurprising effectiveness of pre-trained vision models for control. In *International Conference on Machine Learning*, pp. 17359–17371. PMLR, 2022.
- Paszke, A., Gross, S., Massa, F., Lerer, A., Bradbury, J., Chanan, G., Killeen, T., Lin, Z., Gimelshein, N., Antiga, L., et al. Pytorch: An imperative style, high-performance deep learning library. *Advances in neural information processing systems*, 32, 2019.
- Pomerleau, D. A. Alvin: An autonomous land vehicle in a neural network. *Advances in neural information processing systems*, 1, 1988.
- Qi, C. R., Su, H., Mo, K., and Guibas, L. J. Pointnet: Deep learning on point sets for 3d classification and segmentation. In *Proceedings of the IEEE conference on computer vision and pattern recognition*, pp. 652–660, 2017.
- Radford, A., Kim, J. W., Hallacy, C., Ramesh, A., Goh, G., Agarwal, S., Sastry, G., Askell, A., Mishkin, P., Clark, J., et al. Learning transferable visual models from natural language supervision. In *International conference on machine learning*, pp. 8748–8763. PMLR, 2021.
- Radosavovic, I., Xiao, T., James, S., Abbeel, P., Malik, J., and Darrell, T. Real-world robot learning with masked visual pre-training. In *Conference on Robot Learning*, pp. 416–426. PMLR, 2023.
- Raghu, M., Unterthiner, T., Kornblith, S., Zhang, C., and Dosovitskiy, A. Do vision transformers see like convolutional neural networks? *Advances in Neural Information Processing Systems*, 34:12116–12128, 2021.
- Schenck, C. and Fox, D. Spnets: Differentiable fluid dynamics for deep neural networks. In *Conference on Robot Learning*, pp. 317–335. PMLR, 2018.
- Shan, D., Geng, J., Shu, M., and Fouhey, D. F. Understanding human hands in contact at internet scale. In *Proceedings of the IEEE/CVF conference on computer vision and pattern recognition*, pp. 9869–9878, 2020.
- Shridhar, M., Manuelli, L., and Fox, D. Cliport: What and where pathways for robotic manipulation. In *Conference on Robot Learning*, pp. 894–906. PMLR, 2022.
- Shridhar, M., Manuelli, L., and Fox, D. Perceiver-actor: A multi-task transformer for robotic manipulation. In *Conference on Robot Learning*, pp. 785–799. PMLR, 2023.
- Smith, L. N. and Topin, N. Super-convergence: Very fast training of neural networks using large learning rates. In *Artificial intelligence and machine learning for multi-domain operations applications*, volume 11006, pp. 369–386. SPIE, 2019.
- Sohn, K., Lee, H., and Yan, X. Learning structured output representation using deep conditional generative models. *Advances in neural information processing systems*, 28, 2015.
- Sutton, R. S. and Barto, A. G. Reinforcement learning: An introduction. *Robotica*, 17(2):229–235, 1999.
- Team, O. M., Ghosh, D., Walke, H., Pertsch, K., Black, K., Mees, O., Dasari, S., Hejna, J., Xu, C., Luo, J., et al. Octo: An open-source generalist robot policy, 2023.
- Wu, X., Wen, X., Liu, X., and Zhao, H. Masked scene contrast: A scalable framework for unsupervised 3d representation learning. In *Proceedings of the IEEE/CVF Conference on Computer Vision and Pattern Recognition*, pp. 9415–9424, 2023.

- Xie, S., Gu, J., Guo, D., Qi, C. R., Guibas, L., and Litany, O. Pointcontrast: Unsupervised pre-training for 3d point cloud understanding. In *Computer Vision–ECCV 2020: 16th European Conference, Glasgow, UK, August 23–28, 2020, Proceedings, Part III 16*, pp. 574–591. Springer, 2020.
- Yadav, K., Ramrakhya, R., Majumdar, A., Berges, V.-P., Kuhar, S., Batra, D., Baevski, A., and Maksymets, O. Offline visual representation learning for embodied navigation. *arXiv preprint arXiv:2204.13226*, 2022.
- Yang, H., He, T., Liu, J., Chen, H., Wu, B., Lin, B., He, X., and Ouyang, W. Gd-mae: generative decoder for mae pre-training on lidar point clouds. In *Proceedings of the IEEE/CVF Conference on Computer Vision and Pattern Recognition*, pp. 9403–9414, 2023a.
- Yang, H., Zhang, S., Huang, D., Wu, X., Zhu, H., He, T., Tang, S., Zhao, H., Qiu, Q., Lin, B., et al. Unipad: A universal pre-training paradigm for autonomous driving. *arXiv preprint arXiv:2310.08370*, 2023b.
- Yen-Chen, L., Zeng, A., Song, S., Isola, P., and Lin, T.-Y. Learning to see before learning to act: Visual pre-training for manipulation. In *2020 IEEE International Conference on Robotics and Automation (ICRA)*, pp. 7286–7293. IEEE, 2020.
- Ze, Y., Yan, G., Wu, Y.-H., Macaluso, A., Ge, Y., Ye, J., Hansen, N., Li, L. E., and Wang, X. Gnfactor: Multi-task real robot learning with generalizable neural feature fields. In *Conference on Robot Learning*, pp. 284–301. PMLR, 2023.
- Zeng, A., Florence, P., Tompson, J., Welker, S., Chien, J., Attarian, M., Armstrong, T., Krasin, I., Duong, D., Sindhvani, V., et al. Transporter networks: Rearranging the visual world for robotic manipulation. In *Conference on Robot Learning*, pp. 726–747. PMLR, 2021.
- Zhang, R., Guo, Z., Gao, P., Fang, R., Zhao, B., Wang, D., Qiao, Y., and Li, H. Point-m2ae: multi-scale masked autoencoders for hierarchical point cloud pre-training. *Advances in neural information processing systems*, 35: 27061–27074, 2022.
- Zhang, T., McCarthy, Z., Jow, O., Lee, D., Chen, X., Goldberg, K., and Abbeel, P. Deep imitation learning for complex manipulation tasks from virtual reality teleoperation. In *2018 IEEE International Conference on Robotics and Automation (ICRA)*, pp. 5628–5635. IEEE, 2018.
- Zhao, T. Z., Kumar, V., Levine, S., and Finn, C. Learning fine-grained bimanual manipulation with low-cost hardware. *arXiv preprint arXiv:2304.13705*, 2023.
- Zhou, T., Tucker, R., Flynn, J., Fyffe, G., and Snavely, N. Stereo magnification: Learning view synthesis using multiplane images. *arXiv preprint arXiv:1805.09817*, 2018.
- Zhou, Y., Barnes, C., Lu, J., Yang, J., and Li, H. On the continuity of rotation representations in neural networks. In *Proceedings of the IEEE/CVF Conference on Computer Vision and Pattern Recognition*, pp. 5745–5753, 2019.
- Zhu, H., Yang, H., Wu, X., Huang, D., Zhang, S., He, X., He, T., Zhao, H., Shen, C., Qiao, Y., et al. Ponderv2: Pave the way for 3d foundation model with a universal pre-training paradigm. *arXiv preprint arXiv:2310.08586*, 2023.

A Task Details and Examples

A.1 Maniskill2

A.1.1 PICKCUBE-V0

- **Objective:** Pick up a cube and move it to a goal position.
- **Success Criteria:** The cube is within 2.5 cm of the goal position, and the robot is static.
- **Demonstration:** 1000 successful trajectories.
- **Oracle Trajectory:** Shown in Figure A.1.

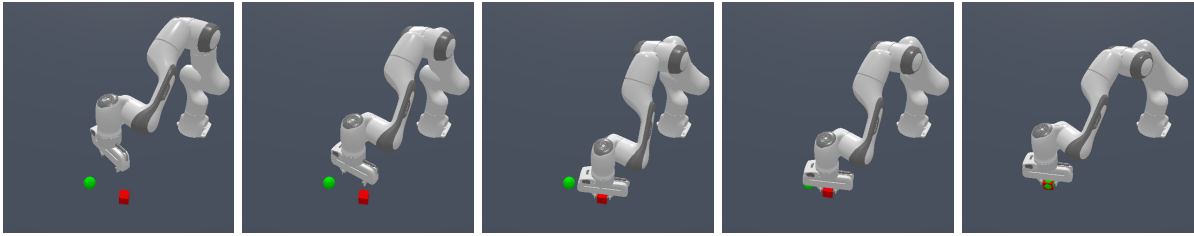


Figure A.1. Illustrations on ManiSkill2 task: PickCube-v0.

A.1.2 STACKCUBE-V0

- **Objective:** Pick up a red cube and place it onto a green one.
- **Success Criteria:** The red cube is placed on top of the green one stably and it is not grasped..
- **Demonstration:** 1000 successful trajectories.
- **Oracle Trajectory:** Shown in Figure A.2.

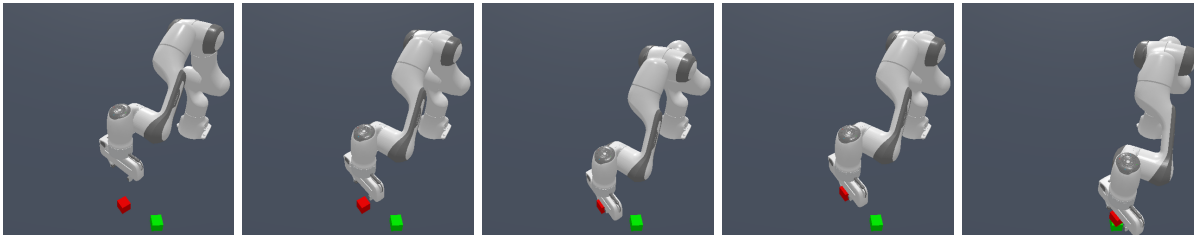


Figure A.2. Illustrations on ManiSkill2 task: StackCube-v0.

A.1.3 TURNFAUCET-V0

- **Objective:** Turn on a faucet by rotating its handle.
- **Success Criteria:** The faucet handle has been turned past a target angular distance.
- **Demonstration:** From the original set of 5510 trajectories (100 trajectories per faucet for most of 60 models from PartNet-Mobility), our experiment focused on 10 models, totaling 1000 trajectories.
- **Oracle Trajectory:** Shown in Figure A.3.

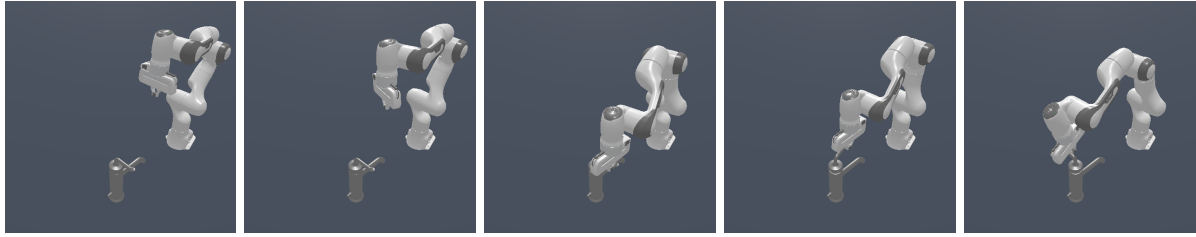


Figure A.3. Illustrations on ManiSkill2 task: TurnFaucet-v0.

A.1.4 PEGINSERTIONSIDE-V0

- **Objective:** Pick up the peg, align it with the horizontal hole in the box, and then insert the peg into the hole.
- **Success Criteria:** The task is segmented into three stages of success. Initially, the peg is picked up. Subsequently, the peg is aligned such that both its head and entirety are within 1 cm of the target hole on the YZ plane. The final stage is achieved when half of the peg is successfully inserted into the hole.
- **Demonstration:** 1000 successful trajectories.
- **Oracle Trajectory:** Shown in Figure A.4.

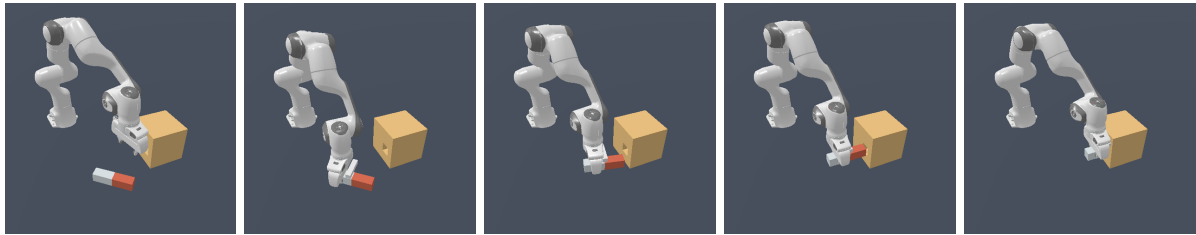


Figure A.4. Illustrations on ManiSkill2 task: PegInsertionSide-v0.

A.1.5 EXCAVATE-V0

- **Objective:** Lift a specific amount of clay to a target height.
- **Success Criteria:** The amount of lifted clay must be within a given range; the lifted clay is higher than a specific height; fewer than 20 clay particles are spilled on the ground; soft body velocity < 0.05 .
- **Demonstration:** 200 successful trajectories.
- **Oracle Trajectory:** Shown in Figure A.5.

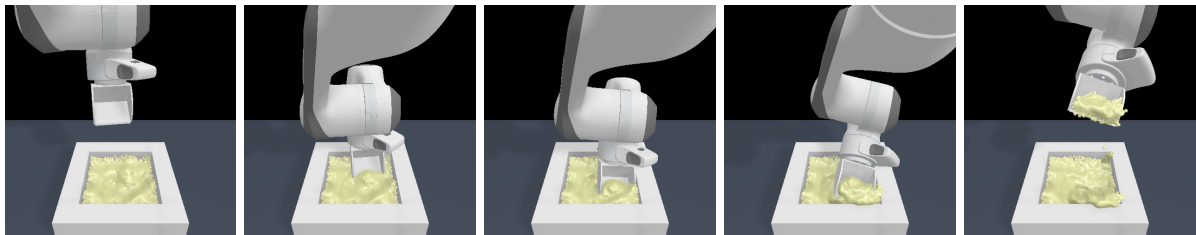


Figure A.5. Illustrations on ManiSkill2 task: Excavate-v0.

A.1.6 HANG-V0

- **Objective:** Hang a noodle on a target rod.
- **Success Criteria:** Part of the noodle is higher than the rod; two ends of the noodle are on different sides of the rod; the noodle is not touching the ground; the gripper is open; soft body velocity < 0.05 .
- **Demonstration:** 200 successful trajectories.
- **Oracle Trajectory:** Shown in Figure A.6.

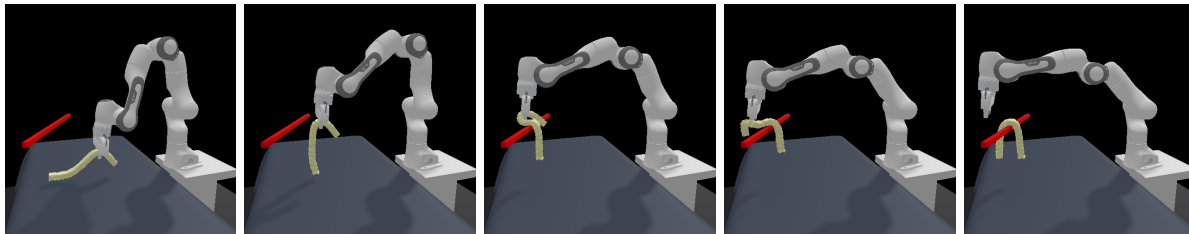


Figure A.6. Illustrations on ManiSkill2 task: Hang-v0.

A.1.7 POUR-V0

- **Objective:** Pour liquid from a bottle into a beaker.
- **Success Criteria:** The liquid level in the beaker is within 4mm of the red line; the spilled water is fewer than 100 particles; the bottle returns to the upright position in the end; robot arm velocity < 0.05 .
- **Demonstration:** 200 successful trajectories.
- **Oracle Trajectory:** Shown in Figure A.7.

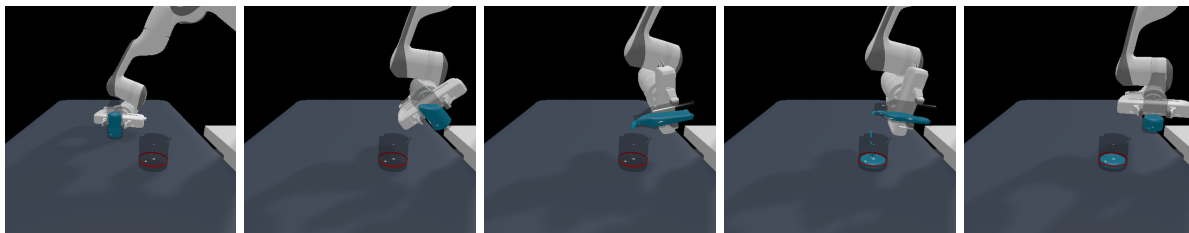


Figure A.7. Illustrations on ManiSkill2 task: Pour-v0.

A.1.8 FILL-V0

- **Objective:** Fill clay from a bucket into the target beaker.
- **Success Criteria:** The amount of clay inside the target beaker $> 90\%$; soft body velocity < 0.05 .
- **Demonstration:** 200 successful trajectories.
- **Oracle Trajectory:** Shown in Figure A.8.

A.2 RLBench

All RLBench tasks are trained on 100 successful trajectories. Each task has multiple variations with different language descriptions.

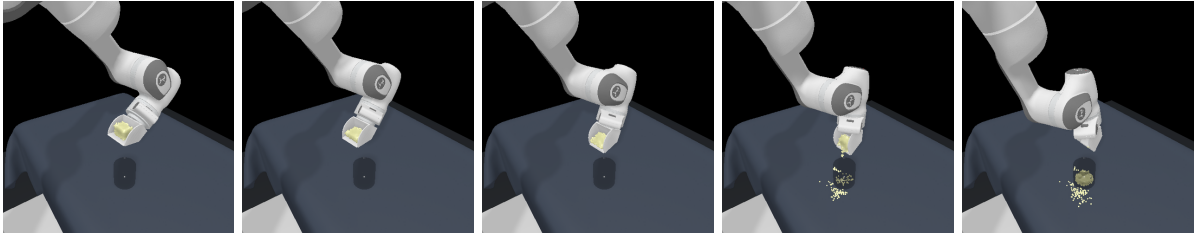


Figure A.8. Illustrations on ManiSkill2 task: Fill-v0.

A.2.1 OPEN DRAWER

- **Objective:** Open one of the three drawers: top, middle, or bottom.
- **Success Criteria:** The prismatic joint of the specified drawer is fully extended.
- **Example description:** Open the top drawer.
- **Oracle Trajectory:** Shown in Figure A.9.

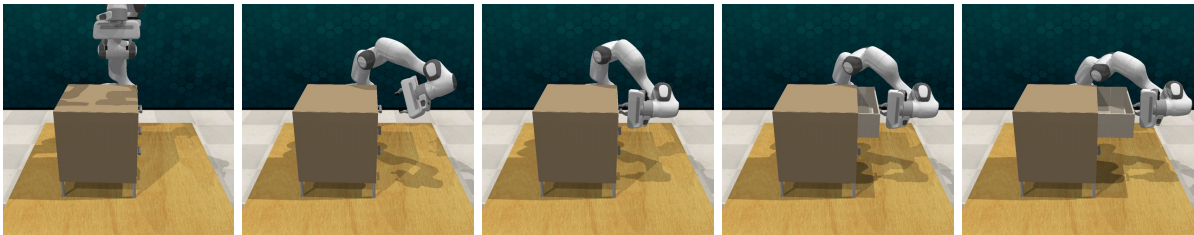


Figure A.9. Illustrations on RLbench task: open drawer.

A.2.2 SWEEP TO DUSTPAN OF SIZE

- **Objective:** Use the broom to brush the dirt particles into either the short or tall dustpan.
- **Success Criteria:** All 5 dirt particles are inside the specified dustpan.
- **Example description:** Sweep dirt to the short dustpan.
- **Oracle Trajectory:** Shown in Figure A.10.

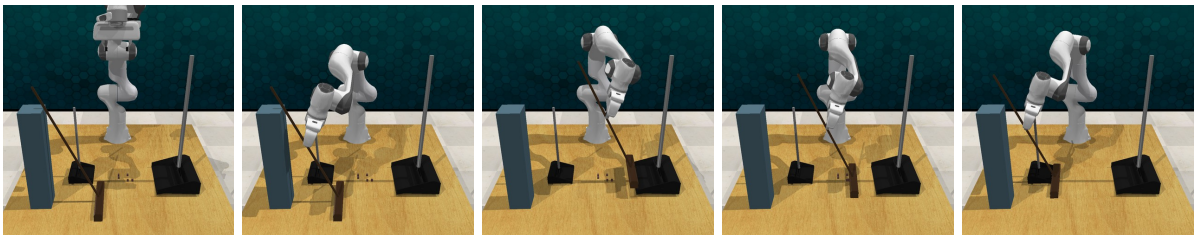


Figure A.10. Illustrations on RLbench task: sweep to dustpan of size.

A.2.3 MEAT OFF GRILL

- **Objective:** Take either the chicken or steak off the grill and set it down on the side.
- **Success Criteria:** The specified meat is on the side, away from the grill.
- **Example description:** Take the steak off the grill.
- **Oracle Trajectory:** Shown in Figure A.11.



Figure A.11. Illustrations on RL Bench task: meat off grill .

A.2.4 TURN TAP

- **Objective:** Turn either the left or right handle of the tap. Left and right are defined with respect to the faucet orientation.
- **Success Criteria:** The revolute joint of the specified handle is at least 90° off from the starting position.
- **Example description:** Turn right tap.
- **Oracle Trajectory:** Shown in Figure A.12.



Figure A.12. Illustrations on RL Bench task: turn tap .

A.2.5 REACH AND DRAG

- **Objective:** Grab the stick and use it to drag the cube on to the specified colored target square. The target colors are sampled from the full set of 20 color instances.
- **Success Criteria:** Some part of the block is inside the specified target area.
- **Example description:** Use the stick to drag the cube onto the navy target.
- **Oracle Trajectory:** Shown in Figure A.13.

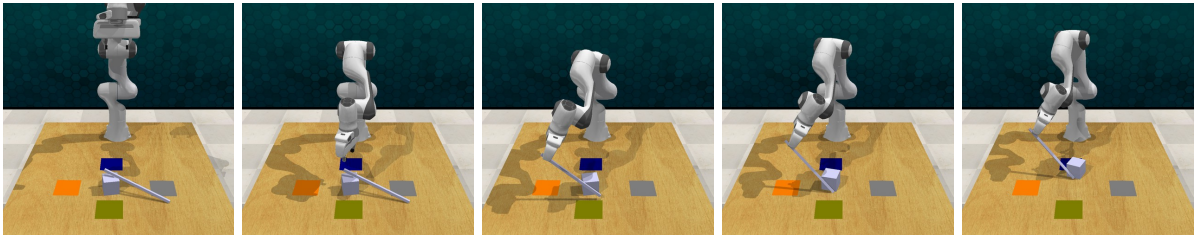


Figure A.13. Illustrations on RL Bench task: reach and drag .

A.2.6 PUT MONEY IN SAFE

- **Objective:** Pick up the stack of money and put it inside the safe on the specified shelf. The shelf has three placement locations: top, middle, bottom.

- **Success Criteria:** The stack of money is on the specified shelf inside the safe.
- **Example description:** Put the money away in the safe on the top shelf.
- **Oracle Trajectory:** Shown in Figure A.14.

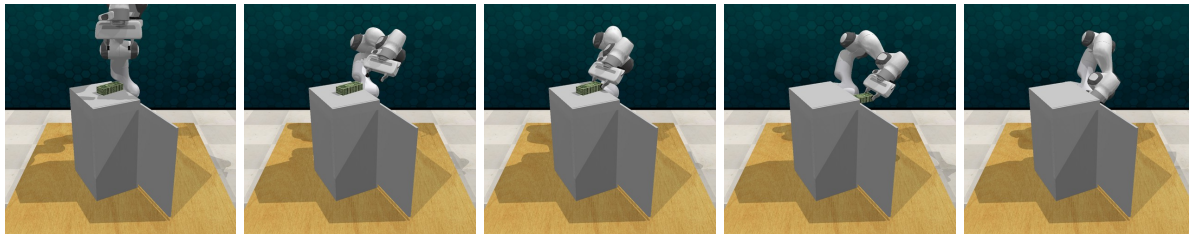


Figure A.14. Illustrations on RL Bench task: put money in safe.

A.2.7 PUSH BUTTONS

- **Objective:** Push the colored buttons in the specified sequence. The button colors are sampled from the full set of 20 color instances. There are always three buttons in scene.
- **Success Criteria:** All the specified buttons were pressed.
- **Example description:** Push the maroon button, then push the green button, then push the navy button.
- **Oracle Trajectory:** Shown in Figure A.15.

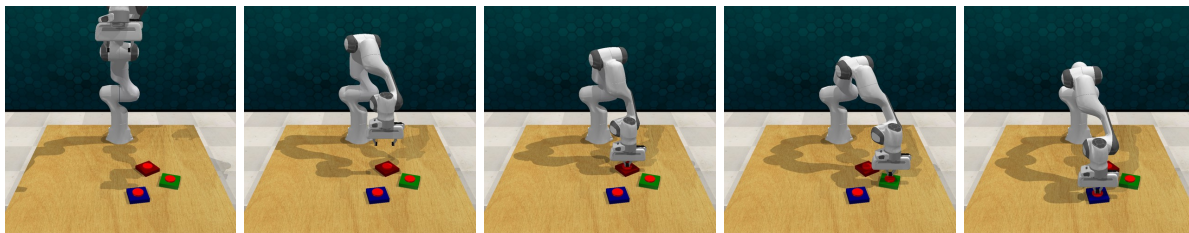


Figure A.15. Illustrations on RL Bench task: push buttons.

A.2.8 CLOSE JAR

- **Objective:** Pick up the lid and close the jar of the specified color. The target colors are sampled from the full set of 20 color instances.
- **Success Criteria:** The lid is capped on a specific jar.
- **Example description:** Close the red jar.
- **Oracle Trajectory:** Shown in Figure A.16.

A.2.9 PLACE WINE AT RACK LOCATION

- **Objective:** Grab the wine bottle and put it on the wooden rack at one of the three specified locations: left, middle, right. The locations are defined with respect to the orientation of the wooden rack.
- **Success Criteria:** The wine bottle is at the specified placement location on the wooden rack.
- **Example description:** Stack the wine bottle to the left of the rack.
- **Oracle Trajectory:** Shown in Figure A.17.

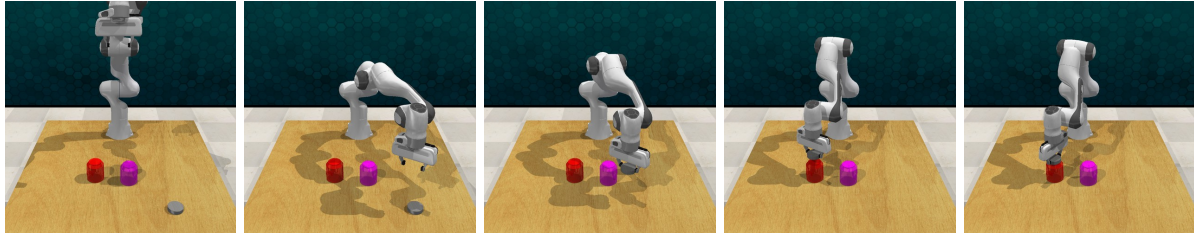


Figure A.16. Illustrations on RL Bench task: close jar.

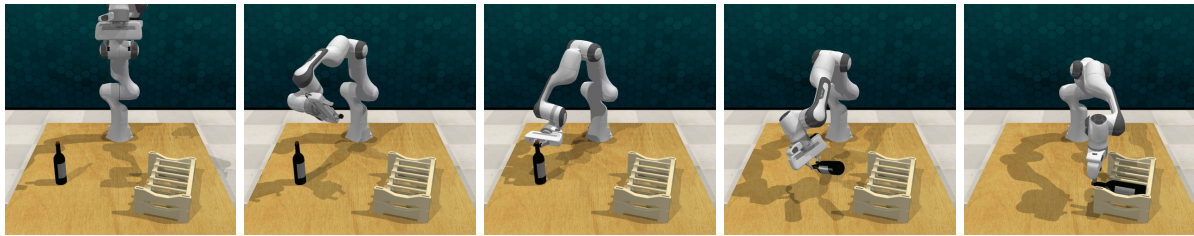


Figure A.17. Illustrations on RL Bench task: place wine at rack location.

B Method Details

B.1 Encoders

- **ResNet50.** A key element in the ◦ ResNet50 (He et al., 2016) architecture is its utilization of deep residual learning with skip connections, a design that effectively addresses the vanishing gradient problem in deep networks. This structure allows ◦ ResNet50 to develop robust feature representations, crucial for complex image processing tasks.
- **ViT-B (Vision Transformer).** Representing a significant shift in image processing, ◦ ViT-B (Dosovitskiy et al., 2020) applies the transformer mechanism, traditionally used in natural language processing, to visual data. It processes images by segmenting them into patches and analyzing these via a transformer encoder, adept at capturing intricate spatial hierarchies.
- **MultiViT-B.** An innovative adaptation of the Vision Transformer, ◦ MultiViT-B (Bachmann et al., 2022) is tailored for multi-modal input, including RGB-D images. It features unique projection layers for each modality, seamlessly integrating depth information with RGB data. This fusion enriches the model’s perception of spatial relationships, enhancing its environmental analysis capabilities.
- **SpUNet34.** In the realm of 3D vision, ◦ SpUNet (Contributors, 2022) is a prominent choice for processing sparse 3D data structures like point clouds. It employs sparse convolution, efficiently handling non-uniform data distribution in 3D space. The SpUNet architecture, inspired by ResNet34, is modified to accommodate the nuances of 3D point cloud data, ensuring effective processing and interpretation of these complex structures.

B.2 Pretrained Visual Representations

- **R3M.** Employed for ◦ ResNet50, • R3M (Nair et al., 2023) uses time-contrastive learning, video-language alignment, and L1 regularization to produce sparse, compact representations. It’s trained on a substantial 3,500 hours of human interaction videos from the Ego4D (Grauman et al., 2022) dataset, demonstrating superior performance over other methods like CLIP (Radford et al., 2021) and MoCo (He et al., 2020) in simulated robotic manipulation tasks.
- **VC-1.** This approach pretrains a ViT using masked auto-encoding (MAE) (He et al., 2022), similar to MVP (Radosavovic et al., 2023) but with a broader dataset range, including Ego4D (Grauman et al., 2022), 100 Days of Hands (100DOH) (Shan et al., 2020), Something-Something v2 (SS-V2) (Goyal et al., 2017), Epic Kitchens (Damen et al., 2018), Real Estate 10K (Zhou et al., 2018), and ImageNet (Deng et al., 2009). It excels in diverse embodied AI tasks.
- **MultiMAE (Multi-modal Multi-task Masked Autoencoders).** • MultiMAE (Bachmann et al., 2022) is utilized for MultiViT, featuring masked autoencoding across various modalities including RGB, depth, and semantics on the ImageNet-1K dataset. Its cross-modality predictive coding significantly enhances transfer to downstream tasks such as image

classification and depth estimation. In our study, we focus on its RGB and depth components.

• **PonderV2.** As the state-of-the-art self-supervised learning method for point clouds, • PonderV2 (Zhu et al., 2023) employs differentiable neural rendering. The method trains a 3D backbone (◦ SpUNet34) within a volumetric neural renderer, focusing on learning detailed geometry and appearance cues. • PonderV2 is effective across a wide range of tasks, including high-level challenges like 3D detection and segmentation, as well as low-level objectives like 3D reconstruction and image synthesis, covering both indoor and outdoor scenarios. It demonstrates the framework’s effectiveness across multiple benchmarks and showcases its potential in advancing 3D foundation models.

B.3 Policy Network

In our study, we implemented the Action Chunking Transformer (ACT) (Zhao et al., 2023) as our primary policy network. This choice was driven by ACT’s proficiency in addressing the inherent challenges of imitation learning, particularly in precision-demanding contexts where errors tend to accumulate progressively.

ACT stands out for its innovative approach to generative modeling over action sequences, significantly improving the robot’s ability to execute complex tasks with heightened accuracy. One of the pivotal features of ACT is its action chunking technique. This involves grouping sequences of actions into cohesive units for execution, effectively shortening the task’s horizon and minimizing the accumulation of errors. This aspect is particularly beneficial for tasks that require detailed, fine-grained manipulations.

Furthermore, ACT integrates a conditional variational autoencoder (CVAE) architecture. This design is adept at accommodating the variability and stochastic nature found in human demonstrations, a common challenge in robot learning. The CVAE framework facilitates the efficient learning of nuanced manipulation skills, a capability that has led ACT to surpass previous methodologies in both simulated and real-world applications.

C Implementation Details

General Implementations. Our implementation leverages PyTorch (Paszke et al., 2019), a powerful framework for deep learning applications. For the ◦ ResNet50 encoder, we utilized the official model available in TorchVision (Marcel & Rodriguez, 2010), aligning with the implementation in • R3M. This approach ensures consistency with the original work in terms of weights and feature extraction. For the ◦ ViT and • VC-1 models, we meticulously adhered to the original implementations. We chose the ViT-base and corresponding VC-1-base models to maintain parameter consistency with other methods used in our study, promoting relative fairness. In the case of ◦ MultiViT and • MultiMAE, our implementation is based on the official ◦ MultiViT-B model. We employed the strongest pretrained weights available in the official repository, pretrained simultaneously on RGB, depth, and semantic modalities, enhancing the model’s robustness and versatility. For ◦ SpUNet and • PonderV2, we adopt the ◦ SpUNet34 architecture as described in the official • PonderV2 paper, ensuring alignment with their proposed methodology and optimizing the model’s performance in handling point cloud data.

Input Preprocessing. For inputs to ◦ ResNet50 and • R3M, we rigorously adhere to the • R3M preprocessing guidelines. This includes resizing images to 224×224 and normalizing them using the ImageNet mean and standard deviation. For ◦ ViT and • VC-1, we follow the • VC-1 preprocessing protocol. This process involves resizing images to 256×256 via bicubic interpolation, center cropping them to 224×224 , and then normalizing with ImageNet mean and std. For ◦ MultiViT and • MultiMAE inputs, we meticulously replicate the original method’s preprocessing. This includes resizing, center cropping, and normalizing the RGB component, along with truncating and normalizing the depth images. For point cloud data, we employ grid sampling with a grid size of 0.005, aligning with the PonderV2 methodology. Notably, the original PonderV2 model utilizes 6-channel inputs (RGB and normals). In our case, given the absence of normal values in robotic data, we substitute XYZ values alongside RGB. Despite this deviation from the original training distribution, we surprisingly find that this approach yields significant performance improvements after end-to-end finetuning.

Feature Extraction. In line with the original ACT implementation, we extract features from the final convolutional layer of ResNet. To enhance these features, we also follow ACT to incorporate 2D cosine position embeddings, enriching the spatial context of the extracted feature map. For ViT and MultiViT, we focus on the [CLS] token, recognized for encapsulating global information of the input. We treat this token as a 1×768 feature map and apply a position embedding approach analogous to that used for ResNet’s features. In processing point cloud data, our initial step involves utilizing Farthest Point Sampling (FPS) to select 2048 seed points. For each seed point, we employ a K-Nearest Neighbors (KNN) algorithm to cluster 16 neighboring points. Subsequently, each cluster undergoes max pooling following a linear projection layer. The

final step entails adding positional embeddings based on the 3D coordinates of the seed points, which enhances the spatial relevance of the extracted features.

ACT Policy Network. In implementing the Action Chunking Transformer (ACT) policy network, we adhere to the original framework while tailoring the encoder forward function to suit our specific needs. Key hyperparameters are chosen as followings: we set the dropout rate to 0.1, number of heads (nhead) to 8, dimension of feedforward network (dim_feedforward) to 32, number of encoder layers to 4, and decoder layers to 7. The hidden dimension (hidden_dim) is fixed at 512, with chunk sizes of 100 for ManiSkill2 and 20 for RL Bench tasks. The latent dimension (latent_dim) is configured to 32, and the weight for the KL divergence loss is set at 10.0. For tasks involving goal conditions, we project the goals into a 512-dimensional space to align with the hidden dimension of the transformer policy. In the case of language-based goals in RL Bench, we employ the language encoder from CLIP to extract a feature vector of 512 dimensions.

Training Details. For training each method, we employ the AdamW (Loshchilov & Hutter, 2017) optimizer, known for its efficiency in weight optimization, with a weight decay set at 0.05. The OneCycle (Smith & Topin, 2019) learning rate scheduler is configured to accelerate the learning process, featuring a pct_start of 0.15, anneal_strategy set to 'cos', div_factor at 100, and final_div_factor at 1000. The scheduler is updated at a step interval frequency of 1. Experiments are conducted across learning rates of $1e-5$, $5e-5$, $1e-4$, each replicated twice to ensure consistency. Performance evaluation relies on the checkpoint with the lowest validation loss. ManiSkill2 experiments are carried out on an NVIDIA RTX 3090 GPU, with a batch size of 16 over 500 epochs. RL Bench experiments are conducted on an NVIDIA A100 GPU. These experiments have a batch size of 32 and also span 500 epochs. We deviate from the quaternion, opting for a 6D rotation (Zhou et al., 2019) representation for rotation actions, following Gervet et al. (2023). In both sets of experiments, we apply action chunking and temporal ensembling with an exponential decay factor of $k = 0.01$, consistent with the original ACT methodology.

D Full Zero-Shot Generalization Results

Here we give out full results on zero-shot generalization experiments.

D.1 Zero-Shot Generalization to Camera View

The results on camera view changes are listed in Tab. 6, Tab. 7, Tab. 8, Tab. 9.

D.2 Zero-Shot Generalization to Visual Changes

The results on visual changes are listed in Tab. 10.

E Full Sample Efficiency Results

Full sample efficiency results on RL Bench are listed in Tab. 11.

Table 6. Full results on zero-shot generalization of scratch encoders to vertical camera view changes.

Tasks	Vertical 5°				Vertical 10°				
	○ ResNet50	○ ViT-B	○ MultiViT-B	○ SpUNet34	○ ResNet50	○ ViT-B	○ MultiViT-B	○ SpUNet34	
<i>ManiSkill2</i>									
PickCube	0.66	0.13	0.02	0.64	0.58	0.03	0.02	0.44	
StackCube	0.32	0.00	0.00	0.21	0.26	0.00	0.00	0.22	
TurnFaucet	0.08	0.06	0.14	0.09	0.09	0.07	0.13	0.09	
PegInsertionSide	Grasp	0.62	0.33	0.15	0.81	0.45	0.27	0.14	0.81
	Align	0.09	0.02	0.00	0.30	0.04	0.02	0.00	0.28
	Insert	0.00	0.00	0.00	0.01	0.00	0.00	0.00	0.01
Excavate	0.00	0.00	0.00	0.00	0.00	0.00	0.00	0.04	
Hang	0.75	0.51	0.81	0.62	0.61	0.33	0.67	0.71	
Pour	0.01	0.00	0.00	0.08	0.01	0.00	0.00	0.06	
Fill	0.29	0.05	0.75	0.53	0.34	0.10	0.76	0.15	
<i>RLBench</i>									
open drawer	0.00	0.00	0.00	0.00	0.00	0.00	0.00	0.12	
sweep to dustpan of size	0.00	0.00	0.00	0.12	0.00	0.00	0.00	0.04	
meat off grill	0.04	0.08	0.00	0.56	0.00	0.00	0.00	0.12	
turn tap	0.08	0.00	0.00	0.00	0.00	0.00	0.00	0.00	
reach and drag	0.00	0.00	0.04	0.28	0.08	0.00	0.00	0.20	
put money in safe	0.08	0.00	0.16	0.32	0.00	0.00	0.08	0.08	
push buttons	0.08	0.00	0.00	0.08	0.04	0.00	0.00	0.04	
close jar	0.00	0.00	0.00	0.00	0.00	0.00	0.00	0.00	
place wine at rack location	0.12	0.00	0.00	0.00	0.04	0.00	0.00	0.00	
Mean Success rate	0.17	0.06	0.11	0.24	0.13	0.04	0.09	0.18	

Table 7. Full results on zero-shot generalization of PVRs to vertical camera view changes.

Tasks	Vertical 5°				Vertical 10°				
	● R3M	● VC-1	● MultiMAE	● PonderV2	● R3M	● VC-1	● MultiMAE	● PonderV2	
<i>ManiSkill2</i>									
PickCube	0.84	0.74	0.52	0.82	0.84	0.71	0.42	0.66	
StackCube	0.29	0.07	0.25	0.37	0.23	0.07	0.18	0.36	
TurnFaucet	0.09	0.06	0.01	0.07	0.11	0.06	0.08	0.07	
PegInsertionSide	Grasp	0.69	0.49	0.61	0.66	0.51	0.37	0.48	0.65
	Align	0.16	0.04	0.09	0.23	0.09	0.03	0.06	0.23
	Insert	0.01	0.00	0.00	0.03	0.00	0.00	0.00	0.03
Excavate	0.00	0.00	0.11	0.13	0.00	0.00	0.12	0.14	
Hang	0.76	0.75	0.81	0.76	0.54	0.68	0.67	0.56	
Pour	0.06	0.02	0.00	0.09	0.03	0.01	0.00	0.06	
Fill	0.38	0.14	0.69	0.80	0.47	0.22	0.70	0.42	
<i>RLBench</i>									
open drawer	0.04	0.00	0.00	0.00	0.00	0.00	0.00	0.00	
sweep to dustpan of size	0.00	0.04	0.28	0.36	0.00	0.00	0.00	0.16	
meat off grill	0.08	0.04	0.00	0.20	0.04	0.00	0.00	0.08	
turn tap	0.04	0.00	0.00	0.00	0.00	0.00	0.00	0.08	
reach and drag	0.12	0.00	0.12	0.24	0.16	0.00	0.04	0.00	
put money in safe	0.00	0.00	0.44	0.48	0.00	0.00	0.16	0.28	
push buttons	0.00	0.00	0.04	0.04	0.00	0.00	0.00	0.00	
close jar	0.00	0.00	0.00	0.04	0.00	0.00	0.00	0.00	
place wine at rack location	0.04	0.00	0.00	0.12	0.04	0.00	0.00	0.12	
Mean Success rate	0.19	0.13	0.21	0.29	0.16	0.11	0.15	0.21	

Table 8. Full results on zero-shot generalization of scratch encoders to horizontal camera view changes.

Tasks	Horizontal 5°				Horizontal 10°				
	○ ResNet50	○ ViT-B	○ MultiViT-B	○ SpUNet34	○ ResNet50	○ ViT-B	○ MultiViT-B	○ SpUNet34	
<i>ManiSkill2</i>									
PickCube	0.65	0.01	0.02	0.70	0.55	0.02	0.03	0.65	
StackCube	0.25	0.00	0.00	0.23	0.01	0.00	0.00	0.09	
TurnFaucet	0.14	0.09	0.13	0.06	0.13	0.09	0.14	0.08	
PegInsertionSide	Grasp	0.52	0.32	0.15	0.81	0.28	0.17	0.15	0.81
	Align	0.11	0.04	0.00	0.27	0.30	0.02	0.01	0.28
	Insert	0.00	0.00	0.00	0.01	0.00	0.00	0.00	0.01
Excavate	0.00	0.00	0.00	0.00	0.00	0.00	0.00	0.00	
Hang	0.81	0.76	0.47	0.79	0.74	0.33	0.45	0.71	
Pour	0.04	0.00	0.00	0.09	0.01	0.00	0.00	0.05	
Fill	0.30	0.08	0.74	0.03	0.31	0.88	0.74	0.02	
<i>RLBench</i>									
open drawer	0.00	0.00	0.00	0.00	0.00	0.00	0.00	0.00	
sweep to dustpan of size	0.24	0.20	0.04	0.80	0.00	0.00	0.08	0.08	
meat off grill	0.16	0.12	0.00	0.48	0.04	0.20	0.00	0.32	
turn tap	0.00	0.00	0.00	0.00	0.04	0.04	0.00	0.00	
reach and drag	0.68	0.36	0.04	0.04	0.32	0.04	0.00	0.00	
put money in safe	0.60	0.32	0.16	0.36	0.24	0.20	0.00	0.24	
push buttons	0.28	0.16	0.08	0.04	0.12	0.08	0.04	0.00	
close jar	0.00	0.00	0.04	0.00	0.00	0.00	0.00	0.00	
place wine at rack location	0.04	0.00	0.00	0.00	0.08	0.00	0.00	0.00	
Mean Success rate	0.25	0.13	0.10	0.25	0.17	0.11	0.09	0.17	

Table 9. Full results on zero-shot generalization of PVRs to horizontal camera view changes.

Tasks	Horizontal 5°				Horizontal 10°				
	● R3M	● VC-1	● MultiMAE	● PonderV2	● R3M	● VC-1	● MultiMAE	● PonderV2	
<i>ManiSkill2</i>									
PickCube	0.82	0.72	0.49	0.85	0.80	0.62	0.44	0.84	
StackCube	0.28	0.05	0.20	0.23	0.00	0.04	0.17	0.09	
TurnFaucet	0.09	0.08	0.11	0.07	0.09	0.70	0.13	0.06	
PegInsertionSide	Grasp	0.15	0.18	0.28	0.65	0.56	0.43	0.55	0.65
	Align	0.00	0.00	0.00	0.02	0.11	0.06	0.10	0.22
	Insert	0.11	0.06	0.10	0.22	0.00	0.00	0.00	0.02
Excavate	0.00	0.00	0.11	0.03	0.00	0.00	0.11	0.07	
Hang	0.84	0.78	0.45	0.77	0.80	0.67	0.46	0.72	
Pour	0.04	0.03	0.00	0.09	0.02	0.01	0.00	0.05	
Fill	0.46	0.11	0.70	0.03	0.02	0.09	0.70	0.02	
<i>RLBench</i>									
open drawer	0.00	0.00	0.00	0.08	0.00	0.04	0.04	0.04	
sweep to dustpan of size	0.28	0.24	0.56	0.72	0.00	0.04	0.24	0.04	
meat off grill	0.16	0.20	0.04	0.76	0.04	0.16	0.00	0.64	
turn tap	0.00	0.00	0.00	0.08	0.00	0.00	0.04	0.04	
reach and drag	0.00	0.16	0.60	0.36	0.00	0.00	0.04	0.32	
put money in safe	0.04	0.32	0.40	0.32	0.04	0.16	0.16	0.04	
push buttons	0.08	0.16	0.08	0.04	0.04	0.12	0.04	0.08	
close jar	0.00	0.04	0.20	0.12	0.00	0.00	0.08	0.16	
place wine at rack location	0.00	0.00	0.00	0.12	0.00	0.00	0.04	0.08	
Mean Success rate	0.18	0.16	0.23	0.29	0.13	0.17	0.18	0.22	

Table 10. Full results on visual change generalization capabilities.

	○ ResNet50	○ ViT-B	○ MultiViT-B	○ SpUNet34	● R3M	● VC-1	● MultiMAE	● PonderV2
<i>lighting intensity</i>								
0.03	0.000	0.000	0.000	0.005	0.000	0.010	0.098	0.000
0.05	0.000	0.000	0.000	0.015	0.00	0.023	0.108	0.003
0.15	0.000	0.000	0.000	0.038	0.003	0.055	0.210	0.058
0.60	0.000	0.000	0.000	0.208	0.003	0.073	0.218	0.253
1.80	0.000	0.000	0.000	0.133	0.000	0.015	0.083	0.093
3.00	0.000	0.000	0.000	0.125	0.000	0.000	0.035	0.075
<i>noise level</i>								
2	0.008	0.000	0.000	0.098	0.003	0.000	0.203	0.163
16	0.008	0.000	0.000	0.120	0.008	0.000	0.215	0.148
32	0.008	0.000	0.000	0.098	0.008	0.050	0.225	0.138
64	0.008	0.000	0.000	0.085	0.002	0.005	0.210	0.150
<i>background color</i>								
R0.2	0.000	0.000	0.000	0.205	0.000	0.008	0.038	0.365
R0.6	0.000	0.000	0.000	0.213	0.000	0.008	0.000	0.330
R1.0	0.000	0.000	0.000	0.218	0.000	0.003	0.000	0.368
G0.2	0.000	0.000	0.000	0.223	0.000	0.025	0.105	0.340
G0.6	0.000	0.000	0.000	0.213	0.000	0.000	0.003	0.343
G1.0	0.000	0.000	0.000	0.218	0.000	0.003	0.000	0.343

Table 11. Full results on sample efficiency.

Tasks	sample 25%				sample 10%			
	○ ResNet50	○ ViT-B	○ MultiViT-B	○ SpUNet34	○ ResNet50	○ ViT-B	○ MultiViT-B	○ SpUNet34
open drawer	0.080	0.000	0.200	0.120	0.000	0.000	0.040	0.000
sweep to dustpan of size	0.000	0.240	0.040	0.040	0.000	0.000	0.000	0.000
meat off grill	0.000	0.000	0.000	0.000	0.000	0.000	0.000	0.000
turn tap	0.000	0.000	0.000	0.000	0.080	0.000	0.000	0.040
reach and drag	0.000	0.000	0.000	0.000	0.000	0.000	0.000	0.000
put money in safe	0.000	0.000	0.000	0.000	0.000	0.000	0.000	0.000
push buttons	0.000	0.120	0.000	0.000	0.000	0.000	0.000	0.000
close jar	0.000	0.000	0.000	0.000	0.000	0.000	0.000	0.000
place wine at rack location	0.000	0.000	0.000	0.000	0.000	0.000	0.000	0.000
Mean Success rate	0.009	0.040	0.027	0.018	0.009	0.000	0.004	0.004
Mean Rank	1.670	1.330	1.110	1.220	0.650	0.650	0.590	0.590
	● R3M	● VC-1	● MultiMAE	● PonderV2	● R3M	● VC-1	● MultiMAE	● PonderV2
open drawer	0.040	0.000	0.000	0.200	0.040	0.000	0.000	0.000
sweep to dustpan_of_size	0.440	0.240	0.200	0.080	0.000	0.000	0.000	0.000
meat off grill	0.000	0.000	0.000	0.000	0.000	0.000	0.000	0.000
turn tap	0.040	0.000	0.000	0.000	0.000	0.000	0.000	0.120
reach and drag	0.040	0.000	0.000	0.040	0.040	0.000	0.000	0.000
put money in safe	0.000	0.000	0.000	0.000	0.000	0.000	0.000	0.000
push buttons	0.040	0.120	0.080	0.040	0.000	0.000	0.000	0.000
close jar	0.000	0.000	0.000	0.000	0.000	0.000	0.000	0.000
place wine at rack_location	0.000	0.000	0.000	0.000	0.000	0.000	0.000	0.000
Mean Success rate	0.067	0.040	0.031	0.040	0.009	0.000	0.000	0.013
Mean Rank	0.154	0.118	0.097	0.096	1.110	1.330	1.330	1.220